Structural Engineering and Mechanics, *Vol. 69, No. 4 (2019) 439-455*
DOI: https://doi.org/10.12989/sem.2019.69.4.439

Thermal, electrical and mechanical buckling loads of sandwich nano-beams made of FG-CNTRC resting on Pasternak's foundation based on higher order shear deformation theory

Ali Ghorbanpour Arani*[1], Mahmoud Pourjamshidian[1a], Mohammad Arefi[1a] and M.R. Ghorbanpour Arani[2]

[1]*Department of Solid Mechanics, Faculty of Mechanical Engineering, University of Kashan, 87317-53153, Kashan, Iran*
[2]*Electrical Engineering Faculty, Amirkabir University of Technology, Tehran, Iran*

(Received October 9, 2018, Revised December 31, 2018, Accepted January 10, 2019)

Abstract. This research deals with thermo-electro-mechanical buckling analysis of the sandwich nano-beams with face-sheets made of functionally graded carbon nano-tubes reinforcement composite (FG-CNTRC) based on the nonlocal strain gradient elasticity theory (NSGET) considering various higher-order shear deformation beam theories (HSDBT). The sandwich nano-beam with FG-CNTRC face-sheets is subjected to thermal and electrical loads while is resting on Pasternak's foundation. It is assumed that the material properties of the face-sheets change continuously along the thickness direction according to different patterns for CNTs distribution. In order to include coupling of strain and electrical field in equation of motion, the nonlocal non-classical nano-beam model contains piezoelectric effect. The governing equations of motion are derived using Hamilton principle based on HSDBTs and NSGET. The differential quadrature method (DQM) is used to calculate the mechanical buckling loads of sandwich nano-beam as well as critical voltage and temperature rising. After verification with validated reference, comprehensive numerical results are presented to investigate the influence of important parameters such as various HSDBTs, length scale parameter (strain gradient parameter), the nonlocal parameter, the CNTs volume fraction, Pasternak's foundation coefficients, various boundary conditions, the CNTs efficiency parameter and geometric dimensions on the buckling behaviors of FG sandwich nano-beam. The numerical results indicate that, the amounts of the mechanical critical load calculated by PSDBT and TSDBT approximately have same values as well as ESDBT and ASDBT. Also, it is worthy noted that buckling load calculated by aforementioned theories is nearly smaller than buckling load estimated by FSDBT. Also, similar aforementioned structure is used to building the nano/micro oscillators.

Keywords: critical buckling load; nonlocal strain gradient theory; high order shear deformation; reinforcement composite

1. Introduction

Stability of structures in presence of various loads is one of important issues in context of mechanical engineering. Since introduction of nano and micro scale problems, some researchers focused on this issue. Critical loads of structures due to various types of loading such as mechanical, thermal, electrical and magnetic loads in small scale problems needs more consideration. Our literature review indicates that various critical loads of sandwich structures in nano scale based on various shear deformation theory has not been mentioned in detail. To justify necessity of present issue, a comprehensive literature review is presented.

The beam is one of the main members in various complex structures that used as column and bridge. Also, in nano and micro usages this member employed as oscillators for various wide applications. In other hand, to develop the beam performance in the buckling, bending and vibration behavior the designers have to make changes to the structures. In recent years, various methods invented and presented for optimize behavior of the beams. Increasing the bending stiffness by using carbon nanotube that suggested by many scholars is one of the main proposals. In the other way, using new properties of the smart materials such as piezoelectricity and flexoelectricity to develop and optimize various behavior of the structure is main method that many of the researchers advised (Talebi *et al.* 2014, Ghasemi *et al.* 2017, Hamdi *et al.* 2017, Hamdia *et al.* 2017, Ghasemi *et al.* 2018, Msekh *et al.* 2018, Vu-Bac *et al.* 2018).

Integration of nano structures with piezoelectric elements leads to an interesting problems in scope of mechanical engineering and nano-electro-mechanical-systems (Marzbanrad *et al.* 2017, Rahmani *et al.* 2017, Wu *et al.* 2017). In recent years, advances in material engineering have led to the emergence of new materials known as carbon nano-tubes reinforcement composite (CNTRC). The behaviors of the beams in various subjects were studied by the researchers in the form of articles and books (Arvin *et al.* 2010, Asghari *et al.* 2010, Reddy 2011, Reddy and El-Borgi 2014). Various beam theories such as the Euler-Bernoulli, Timoshenko or first order shear deformation (FOSD), Reddy or parabolic shear deformation (PSD) and Levinson beam theories were employed based on

∗Corresponding author, Professor
E-mail: aghorban@kashanu.ac.ir
[a]Ph.D.

http://www.techno-press.com/journals/sem&subpage=7
ISSN: 1225-4568 (Print), 1598-6217 (Online)

the nonlocal differential constitutive relations of Eringen by Reddy (Reddy 2007, El-HakimKhalil *et al.* 2016, Eltaher *et al.* 2016, Mirzabeigy and Madoliat 2016, Ziaee 2016). There are some other theories in relation to beams such as trigonometric shear deformation beam theory (TSDBT), exponential shear deformation beam theory (ESDBT), hyperbolic shear deformation beam theory (HSDBT), and Aydogdu shear deformation beam theory (ASDBT) (Simsek and Reddy 2013, Ansari *et al.* 2016, Gui-Lin *et al.* 2017).

In order to investigate the stability response and buckling analysis of SWCNT embedded in an elastic medium, nonlocal elasticity and Timoshenko beam theory were implemented by Murmu and Pradhan (2009). They used both Winkler-type and Pasternak-type foundation models to simulate the interaction of the (SWCNT) with the surrounding elastic medium. According to their obtained results, the critical buckling loads of SWCNT were strongly dependent on the nonlocal small-scale coefficients and on the stiffness of the surrounding medium. Ansari and Sahmani were proposed a non-classical solution to analyze bending and buckling responses of nano-beams including surface stress effects (Ansari and Sahmani 2011). They evaluated the surface stress effects on the displacement profile and critical buckling load of the nano-beams in each type of beam theory. Numerical results presented in conclusions of aforementioned investigation indicated that the difference between the behaviors of the nano-beam predicted by the classical and non-classical solutions which depends on the magnitudes of the surface elastic constants. An analytical approach for buckling analysis and smart control of a single layer graphene sheet (SLGS) using a coupled polyvinylidene fluoride (PVDF) nano-plate investigated by Ghorbanpour Arani *et al.* (2012). Their results depicted that the imposed voltage is an effective controlling parameter for buckling of the SLGS. Yas and Samadi studied free vibrations and buckling analysis of nano-composite Timoshenko beams reinforced by single-walled carbon nanotubes (SWCNTs) resting on an elastic foundation (Yas and Samadi 2012). In aforementioned investigation it is assumed that the SWCNTs aligned and straight with a uniform layout in whole uniform and three types of functionally graded distributions of CNTs through the thickness. The results obtained in the mentioned investigation indicated that the CNTs distribution play a very important role on the free vibrations and buckling characteristics of the beam. The bending, buckling and vibration behaviors of carbon nanotube-reinforced composite (CNTRC) beams are investigated by Wattanasakulpong and Ungbhakorn (Wattanasakulpong and Ungbhakorn 2013). They presented new results of bending, buckling and vibration analyses of CNTRC beams based on several higher-order shear deformation theories and also discussed in details.

Simsek and Yurtcu examined static bending and buckling of a functionally graded (FG) nano-beam based on the nonlocal Timoshenko and Euler-Bernoulli beam theory (Simsek and Yurtcu 2013). They evaluated and discussed the effects of nonlocal parameter, aspect ratio, various material compositions on the static and stability responses of the FG nano-beam. Based on the modified couple stress theory (MCST), a unified higher order beam theory which contains various beam theories as special cases was proposed by Simsek and Reddy for buckling of a functionally graded (FG) micro-beam embedded in elastic Pasternak medium (Simsek and Reddy 2013). An analytical study on the buckling of double-nano-plate-system (DNPS) subjected to biaxial compression using nonlocal elasticity theory were studied by Murmu *et al.* (2013). According to results obtained in aforementioned investigation the buckling load decreased with increase of value of nonlocal parameter or scale coefficient. Also, the study indicated that the increase of stiffness parameter brings uniaxial and biaxial buckling phenomenon closer while increase of aspect ratio widen uniaxial and biaxial buckling phenomenon. Niknam and Aghdam attempted to obtain a closed form solution for both natural frequency and buckling load of nonlocal FG beams resting on nonlinear elastic foundation (Niknam and Aghdam 2015). They concluded that considering the nonlocal effects decreases the buckling load as well as natural frequency. In addition, according to results presented in the aforementioned study the effects of nonlocal parameters on fully clamped beams are more than other types of boundary conditions. In other investigation, the buckling behavior of orthotropic rectangular nano-plate was studied by Mohammadi *et al.* (Mohammadi *et al.* 2014). In mentioned study, nonlocal elasticity theory was been implemented to investigate the shear buckling of orthotropic single-layered graphene sheets (SLGSs) in thermal environment. Grygorowicz *et al.* studied the analytical and numerical elastic buckling of a three-layered beam with metal foam core (Grygorowicz *et al.* 2015).

Wu and Kitipornchai investigated the free vibration and elastic buckling of sandwich beams with a core and functionally graded carbon nanotube reinforced composite (FG-CNTRC) face sheets within the framework of Timoshenko beam theory (Wu and Kitipornchai 2015). The modified strain gradient (MSG) Reddy rectangular plate theory was extended by Mohammadimehr *et al.* for biaxial buckling and bending analysis of double-coupled polymeric nano-composite plates reinforced by functionally graded single-walled boron nitride nanotubes (FG-SWBNNTs) and functionally graded single-walled carbon nanotubes (FG-SWCNTs) (Mohammadimehra *et al.* 2016). Shafiei and Kazemi presented an exhaustive analysis on the buckling behavior of two-dimensional functionally graded (2D-FG) tapered Euler-Bernoulli beams made of porous materials in nano- and micro-scales (Shafiei and Kazemi 2017). They concluded that Increment of FG power indexes along thickness (nz) and along axis (nx) decrease the buckling load. In the other research, Kameswara Rao and Bhaskara Rao presented the post-buckling behavior of thin-walled beam of open section supported by Winkler-Pasternak foundation subjected to an axial compressive load (Kameswara Raoa and Bhaskara Rao 2017). Zhu *et al.* adopted Eringen's two-phase nonlocal integral model to carry out an analytical study on the buckling problem of Euler-Bernoulli beams (Zhu *et al.* 2017). According to results presented in mentioned study, the nonlocal effect reduced the buckling loads and also the effect could be first-

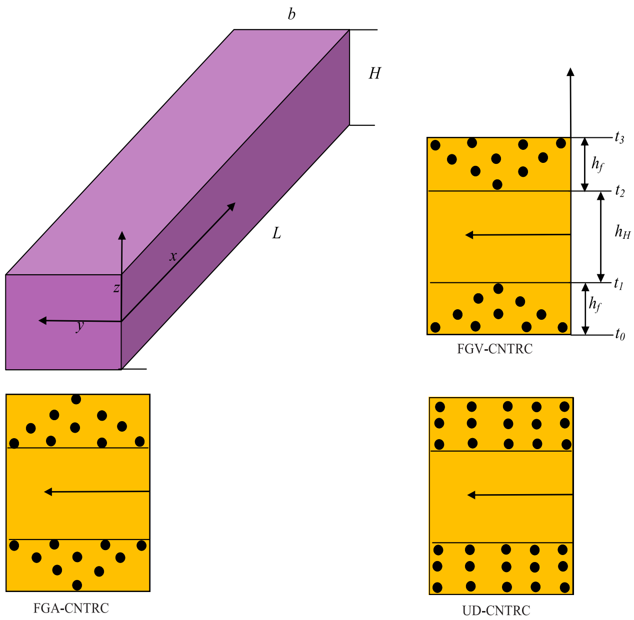

Fig. 1 Sandwich nano-beam with CNTRC face-sheets and attached coordinate system

order or second order depending on the boundary conditions.

With attention to literature review mentioned above and author's knowledge, we can conclude that there is no published work about thermo-electro-mechanical buckling analysis of the sandwich nano-beams with face-sheets made of FG-CNTRC based on NSGET considering various HSDBTs. The sandwich nano-beam with FG-CNTRC face-sheets is subjected to thermal and electrical loads. In this study it is assumed that the material properties of the face-sheets change continuously in the thickness direction according to different patterns for CNTs distribution. The effects of piezoelectricity to consider coupling of strain and electrical field, various HSDBTs, NSGET, and Hamilton's principle are used to derive governing equations of motion. Then DQM is used to calculate the critical buckling mechanical loads of sandwich nano-beam as well as critical buckling applied voltage and increment temperature. Furthermore, the comprehensive numerical results are presented to investigate the influence of important parameters such as various HSDBTs, length scale parameter (strain gradient parameter), nonlocal parameter, volume fraction of the CNTs, Pasternak foundation parameters, various boundary conditions, the CNTs efficiency parameter, and geometric dimensions on the buckling behaviors of FG sandwich nano-beam.

2. Material properties of sandwich FG-CNTRC nano-beams

In this section, the schematic of problem is showed in Fig. 1 and a special consideration is accomplished to the material properties of sandwich nano beam and face-sheets. As can be seen in figure it is clear that the face-sheets are made from CNTRC that in which matrix is piezoelectric. Also, the core of the sandwich nano-beam is only fabricated by piezoelectric materials. Also, this can be seen the CNTs are aligned along thickness direction of the face-sheets with three patterns named $\mathbf{FG(AV)}$, $\mathbf{FG(VA)}$ and $\mathbf{UD}$.

If we consider one element of the composite materials with the overall volume W, the following expression can be written between the volume of the reinforcing phase W_{CN} and matrix W_m as (Tornabene *et al.* 2016, Fantuzzi *et al.* 2017, Tornabene *et al.* 2017)

$$W = W_{CN} + W_m \tag{1}$$

Also, it is worthy noted that the mass fraction of nanoparticles w_{CN} and the mass fraction of the polymer matrix w_m are calculated as the following form (Tornabene *et al.* 2016)

$$w_{CN} = \frac{M_{CN}}{M_{CN} + M_m}, \qquad w_m = \frac{M_m}{M_{CN} + M_m}, \tag{2}$$

In which, M_{CN} and M_m characterize the CNTs and the matrix masses, respectively. At this point, the volume fraction of the CNTs and matrix is defined as

$$V_{CN} = \frac{W_{CN}}{W}, \qquad V_m = \frac{W_m}{W}, \tag{3}$$

The Mori-Tanaka scheme or the rule of mixtures are employed to calculate the effective properties of CNTRC (Tornabene *et al.* 2019, Natarajani *et al.* 2014). In order to improve calculation of the effective material properties of face-sheets made of CNTRC, the rule of mixtures with correction factors is used in this study. Therefore, some of the main CNTRC properties such as Young's modulus (E^{rc}), expansion coefficient (α^{rc}) and density (ρ^{rc}) are calculated based on rule of mixtures with correction factors as the following form (Rafiee *et al.* 2014, Rabani Bidgoli *et al.* 2015, Madani *et al.* 2016)

$$\begin{aligned} E_{11}^{rc} &= \eta_1 V_{cn} E_{11}^{CN} + V_m E^m \\ \frac{\eta_2}{E_{22}^{rc}} &= \frac{V_{CN}}{E_{22}^{CN}} + \frac{V_m}{E^m} \\ \frac{\eta_3}{G_{12}^{rc}} &= \frac{V_{CN}}{G_{12}^{CN}} + \frac{V_m}{G^m} \\ \alpha^{rc} &= V_{cn}\alpha_{11}^{CN} + V_m \alpha^m \\ \rho^{rc} &= V_{cn}\rho^{CN} + V_m \rho^m \end{aligned} \tag{4}$$

where, $\eta_i, (i = 1,2,3)$, E_{ii}^{CN}, G^{CN}, α_{11}^{CN}, and ρ_{11}^{CN} are the CNT efficiency parameter, the Young's modulus, the shear modulus, the expansion coefficient, the visco-elastic coefficient and density of the CNTs, respectively and E^m, G^m, α^m, and ρ^m are the corresponding properties for the matrix. It is worthy noted that in whole of this context superscript rc and m symbolize the reinforcement composite and matrix, respectively. also, volume fraction of CNTs (V_{CN}) and volume fraction of matrix (V_m) are related by this relation $V_{CN} + V_m = 1$ (Shen and Zhang 2012, Tornabene *et al.* 2017). In addition, regarding to studies performed by Tornabene *et al.* (Tornabene *et al.* 2016, Fantuzzi *et al.* 2017, Tornabene *et al.* 2017) if the through the thickness distribution is represented by V_{CN}^d, the gradual variation of the nanoparticles along the normal direction $\bar{z}$ for every layer is given by

$$V_{CN} = V_{CN}^* V_{CN}^d \tag{5}$$

Where, V_{CN}^* can be calculated as the following form

$$V_{CN}^* = \frac{w_{CN}}{w_{CN} + \left(\frac{\rho^{CN}}{\rho^m}\right) - \left(\frac{\rho^{CN}}{\rho^m}\right) w_{CN}} \tag{6}$$

It is very important noted that there is no limitation on the choice of V_{CN}^d because of the aforementioned approach is general, (Allahkarami *et al.* 2017, Fantuzzi *et al.* 2017). Therefore, in present study, the distribution of the CNTs along the face-sheets are given by

$$\begin{aligned}
&V_{CN}^t = 2\frac{(t_2 - \bar{z})}{(t_2 - t_3)} V_{CN}^* \\
&V_{CN}^b = 2\frac{(t_1 + \bar{z})}{(t_1 - t_0)} V_{CN}^*, \quad \Rightarrow \quad \text{for } FG(VA) \text{ pattern} \\
&V_{CN}^t = 2V_{CN}^* \\
&V_{CN}^b = 2V_{CN}^*, \quad \Rightarrow \quad \text{for } UD \text{ pattern} \\
&V_{CN}^t = 2\frac{(t_3 - \bar{z})}{(t_3 - t_2)} V_{CN}^* \\
&V_{CN}^b = 2\frac{(t_0 + \bar{z})}{(t_0 - t_1)} V_{CN}^*, \quad \Rightarrow \quad \text{for } FG(AV) \text{ pattern}
\end{aligned} \tag{7}$$

In which V_{CN}^t and V_{CN}^b represent the volume fractions of the CNTs in top and bottom face-sheets, respectively.

3. Formulation

As mentioned before, higher-order shear deformation beam theory (HSDBT) is used for displacement field of beam as

$$\begin{aligned}
&\bar{u}(\bar{x},\bar{z},\bar{t}) = u_0(\bar{x},\bar{t}) - \bar{z}\frac{\partial w_0(\bar{x},\bar{t})}{\partial \bar{x}} + \varphi(\bar{z})\gamma(\bar{x},\bar{t}) \\
&\bar{w}(\bar{x},\bar{z},\bar{t}) = w_0(\bar{x},\bar{t})
\end{aligned} \tag{8}$$

In above equation, $\bar{u}$ and $\bar{w}$ are axial and transverse displacement components, u_0 and w_0 are axial and transverse displacement of mid-surface. In addition $\varphi(\bar{z})$ is a function of $\bar{z}$ that presents the transverse shear and stress distribution along the thickness of the beam (Simsek and Reddy 2013). Selection of $\varphi(\bar{z})$ is based on various HSDBTs as follows (Meiche *et al.* 2011, Tounsi *et al.* 2013, Belabed *et al.* 2014, Hebali *et al.* 2014, Li *et al.* 2014, Mahi *et al.* 2015, Arefi and Zenkour 2017a, b, c, d, e, f)

$\varphi(\bar{z})$	Theory
$\bar{z}$	FSDBT or Timoshenko
$\bar{z}\left(1-\frac{4\bar{z}^2}{3h^2}\right)$	PSDBT
$\frac{h}{\pi}\sin\left(\frac{\pi\bar{z}}{h}\right)$	TSDBT
$h\sin\left(\frac{\bar{z}}{h}\right) - \bar{z}\cosh\left(\frac{1}{2}\right)$	HSDBT
$\bar{z}\exp\left(-2\left(\frac{\bar{z}}{h}\right)^2\right)$	ESDBT
$\bar{z}\alpha^{\frac{-2\left(\frac{\bar{z}}{h}\right)^2}{\ln\alpha}}$ in which $\alpha = 3$	ASDBT

(9)

Also in Eq. (8), $\gamma(\bar{x},\bar{t})$ is the transverse shear strain of any point on the neutral axis (Simsek and Reddy 2013) and is specified as

$$\gamma(\bar{x},\bar{t}) = \phi(\bar{x},\bar{t}) + \frac{\partial w_0(\bar{x},\bar{t})}{\partial \bar{x}} \tag{10}$$

In Eq. (10), $\phi(\bar{x},\bar{t})$ is the total bending rotation of the cross sections at any point on the neutral axis. The linear strain-displacement relation considering the thermal strain is expressed as

$$\begin{aligned}
&\varepsilon_{\bar{x}\bar{x}} = \frac{\partial u_0}{\partial \bar{x}} - \bar{z}\frac{\partial^2 w_0}{\partial \bar{x}^2} + \varphi\left(\frac{\partial^2 w_0}{\partial \bar{x}^2} - \frac{\partial \phi}{\partial \bar{z}}\right) - \alpha(\bar{z})\Delta T \\
&\varepsilon_{\bar{x}\bar{z}} = \frac{\partial \varphi}{\partial \bar{z}}\left(\frac{\partial w_0}{\partial \bar{x}} - \phi\right)
\end{aligned} \tag{11}$$

In which, ΔT is the increment of temperature from the initial temperature (T_0) that is equal to $\Delta T = T - T_0$. In the present study, it is assumed that the electric potential as a sum of a cosine and linear variation. Then the electric potential can be written as (Arefi *et al.* 2017, Arefi and Zenkour 2017a, b, c, d, e)

$$\tilde{\Phi}(\bar{x},\bar{z},\bar{t}) = \cos(\beta\bar{z})\bar{\Phi}(\bar{x},\bar{t}) + \frac{2\bar{z}V_0}{h} \tag{12}$$

In Eq. (12), $\beta = \frac{\pi}{h}$ and $\bar{\Phi}(\bar{x},\bar{t})$ is electric potential distribution along the longitudinal direction (Ke, Yang *et al.* 2010), V_0 is the applied electric potential (Liew, Yang *et al.* 2003). It is noted that $\bar{\Phi}(\bar{x},\bar{t})$ must satisfy the homogeneous electric boundary conditions. Regard to Eq. (12), the electric fields can be defined as (Arefi *et al.* 2017, Arefi and Zenkour 2017a, b, c, d, e, Arefi 2016)

$$\begin{aligned}
&E_{\bar{x}} = -\frac{\partial \tilde{\Phi}}{\partial \bar{x}} = -\cos(\beta\bar{z})\frac{\partial \bar{\Phi}}{\partial \bar{x}} \\
&E_{\bar{z}} = -\frac{\partial \tilde{\Phi}}{\partial \bar{z}} = \beta\sin(\beta\bar{z})\bar{\Phi}(\bar{x},\bar{t}) - E_0, \quad E_0 = \frac{2V_0}{h}
\end{aligned} \tag{13}$$

The strain-stress relation for reinforcement composite face-sheets defined as (Li *et al.* 2015)

$$\begin{aligned}&\sigma_{\bar{x}\bar{x}}^{f}=E^{f}\left(\bar{z}\right)\left(\frac{\partial u_0}{\partial \bar{x}}-\bar{z}\frac{\partial^2 w_0}{\partial \bar{x}^2}+\varphi\left(\frac{\partial^2 w_0}{\partial \bar{x}^2}-\frac{\partial \phi}{\partial \bar{z}}\right)-\alpha\left(\bar{z}\right)\Delta T\right)\\&\sigma_{\bar{x}\bar{z}}^{f}=G^{f}\left(\bar{z}\right)\frac{\partial \varphi}{\partial \bar{z}}\left(\frac{\partial w_0}{\partial \bar{x}}-\phi\right)\end{aligned}\tag{14}$$

In general, the properties associated with the core and face-sheets represent with p and f superscripts, respectively. In addition, the constitutive relations for piezoelectric core layer are specified as

$$\begin{aligned}&\sigma_{\bar{x}\bar{x}}^{p}=E^{p}\left(\frac{\partial u_0}{\partial \bar{x}}-\bar{z}\frac{\partial^2 w_0}{\partial \bar{x}^2}+\varphi\left(\frac{\partial^2 w_0}{\partial \bar{x}^2}-\frac{\partial \phi}{\partial \bar{z}}\right)-\alpha\left(\bar{z}\right)\Delta T\right)-e_{31}E_{\bar{z}}\\&\sigma_{\bar{x}\bar{z}}^{p}=G^{p}\frac{\partial \varphi}{\partial \bar{z}}\left(\frac{\partial w_0}{\partial \bar{x}}-\phi\right)-e_{15}E_{\bar{x}}\\&D_{\bar{x}}=e_{15}\varepsilon_{\bar{x}\bar{z}}-k_{11}E_{\bar{x}}\\&D_{\bar{z}}=e_{31}\varepsilon_{\bar{x}\bar{x}}-k_{33}E_{\bar{z}}\end{aligned}\tag{15}$$

In which, $D_{\bar{x}}$ and $D_{\bar{z}}$ represent the electric displacement. In addition, e_{31}, e_{15} are the piezoelectric constants and k_{11}, k_{33} are the dielectric constants (Liew *et al.* 2003, Rafiee *et al.* 2013). The Hamilton's principle is used to drive governing equation of motion as (Komijani *et al.* 2014)

$$0=\int_0^T\left(\delta T-\delta U_s-\delta U_f+\delta W\right)d\bar{t}\tag{16}$$

Where δU_s, δU_f, δT and δW are the variations of strain energy, reaction of foundation, kinetic energy and works due to external works, respectively. Variation of strain energy δU_s is calculated as

$$\delta U_s=\int_0^L\int_A\left(\sigma_{\bar{x}\bar{x}}\delta\varepsilon_{\bar{x}\bar{x}}+\sigma_{\bar{x}\bar{z}}\delta\varepsilon_{\bar{x}\bar{z}}-D_{\bar{x}}E_{\bar{x}}-D_{\bar{z}}E_{\bar{z}}\right)dA\,d\bar{x}\tag{17}$$

Variation of kinetic energy is represented as

$$\delta T=\int_0^L\int_A\rho\left(\bar{z}\right)\left(\frac{\partial \bar{u}}{\partial \bar{t}}\frac{\partial \bar{u}}{\partial \bar{t}}+\frac{\partial \bar{w}}{\partial \bar{t}}\frac{\partial \bar{w}}{\partial \bar{t}}\right)dA\,d\bar{x}\tag{18}$$

Variations of work done by the forces and the nonlinear elastic foundation are written as (Ghorbanpour Arani *et al.* 2012, Kanani *et al.* 2014, Komijani *et al.* 2014)

$$\begin{aligned}&\delta W=\int_0^L\left(F\delta u_0+Q\delta w_0+\bar{N}_0\frac{\partial w_0}{\partial \bar{x}}\frac{\partial \delta w_0}{\partial \bar{x}}\right)d\bar{x}\\&\delta U_f=\int_0^L\int_0^b\left(\bar{K}_w w_0\delta w_0+\bar{K}_s\frac{\partial w_0}{\partial \bar{x}}\delta\left(\frac{\partial w_0}{\partial \bar{x}}\right)\right)d\bar{y}\,d\bar{x}\end{aligned}\tag{19}$$

Where F and Q are the axial and transverse forces per unit length respectively and $\bar{N}_0$ is the axial compressive or pretension force. Also, $\bar{K}_w$ and $\bar{K}_s$ are linear spring and shear coefficients of foundation, respectively. Substituting Eqs. (8)-(11) into Eqs. (17)-(19) and consequently into Eq. (16), yields the governing equations of motions as

$$\begin{aligned}&\delta u_0:\ \frac{\partial N_{\bar{x}}}{\partial \bar{x}}+F=\bar{I}_A\frac{\partial^2 u_0}{\partial \bar{t}^2}-\bar{I}_{B1}\frac{\partial^3 w_0}{\partial \bar{t}^2\partial \bar{x}}+\bar{I}_{B2}\frac{\partial^3 w_0}{\partial \bar{t}^2\partial \bar{x}}-\bar{I}_{B2}\frac{\partial^2 \phi}{\partial \bar{t}^2}\\[6pt]&\delta w_0:\ \frac{\partial^2 M_{\bar{x}}}{\partial \bar{x}^2}-\frac{\partial^2 M_{\bar{x}}^{h}}{\partial \bar{x}^2}+\frac{\partial}{\partial \bar{x}}\left(N_{\bar{x}}\frac{\partial w_0}{\partial \bar{x}}\right)+\frac{\partial Q_{\bar{x}\bar{z}}}{\partial \bar{x}}-\bar{K}_w w_0+\bar{K}_s\frac{\partial^2 w_0}{\partial \bar{x}^2}+\bar{N}_0\frac{\partial^2 w_0}{\partial \bar{x}^2}+Q=\bar{I}_{B1}\frac{\partial^3 u_0}{\partial \bar{x}\partial \bar{t}^2}-\\&\qquad\bar{I}_{B2}\frac{\partial^3 u_0}{\partial \bar{x}\partial \bar{t}^2}+\bar{I}_A\frac{\partial^2 w_0}{\partial \bar{t}^2}-\bar{I}_{D1}\frac{\partial^4 w_0}{\partial \bar{t}^2\partial \bar{x}^2}+\bar{I}_{D2}\frac{\partial^4 w_0}{\partial \bar{t}^2\partial \bar{x}^2}+\bar{I}_{D2}\frac{\partial^4 w_0}{\partial \bar{t}^2\partial \bar{x}^2}-\bar{I}_{D3}\frac{\partial^4 w_0}{\partial \bar{t}^2\partial \bar{x}^2}-\bar{I}_{D2}\frac{\partial^3 \phi}{\partial \bar{x}\partial \bar{t}^2}+\bar{I}_{D3}\frac{\partial^3 \phi}{\partial \bar{x}\partial \bar{t}^2}\\[6pt]&\delta\phi:\ Q_{\bar{x}\bar{z}}-\frac{\partial M_{\bar{x}}}{\partial \bar{x}}=\bar{I}_{B2}\frac{\partial^2 u_0}{\partial \bar{t}^2}+\bar{I}_{D2}\frac{\partial^3 w_0}{\partial \bar{t}^2\partial \bar{x}}-\bar{I}_{D3}\frac{\partial^3 w_0}{\partial \bar{t}^2\partial \bar{x}}+\bar{I}_{D3}\frac{\partial^2 \phi}{\partial \bar{t}^2}\\[6pt]&\delta\xi:\ \int_A\left(\cos\left(\beta\bar{z}\right)\frac{\partial \bar{D}_{\bar{x}}}{\partial \bar{x}}-\beta\sin\left(\beta\bar{z}\right)\bar{D}_{\bar{z}}\right)dA=0\end{aligned}\tag{20}$$

Where, $N_{\bar{x}}$, $Q_{\bar{x}\bar{z}}$, $M_{\bar{x}}$ and $M_{\bar{x}}^{h}$ the resultants of forces and the moments. They are expressed as

$$\begin{aligned}&N_{\bar{x}}=\int_{-h/2}^{h/2}\sigma_{\bar{x}\bar{x}}\left(\bar{z}\right)d\bar{z}=\left(\int_{t_0}^{t_1}\sigma_{\bar{x}\bar{x}}^{f}d\bar{z}+\int_{t_1}^{t_2}\sigma_{\bar{x}\bar{x}}^{p}d\bar{z}+\int_{t_2}^{t_3}\sigma_{\bar{x}\bar{x}}^{f}d\bar{z}\right)\\&Q_{\bar{x}\bar{z}}=\int_{-h/2}^{h/2}\frac{\partial\varphi\left(\bar{z}\right)}{\partial \bar{x}}\sigma_{\bar{x}\bar{z}}\left(\bar{z}\right)d\bar{z}=\\&\quad\left(\int_{t_0}^{t_1}\frac{\partial\varphi\left(\bar{z}\right)}{\partial \bar{x}}\sigma_{\bar{x}\bar{x}}^{f}d\bar{z}+\int_{t_1}^{t_2}\frac{\partial\varphi\left(\bar{z}\right)}{\partial \bar{x}}\sigma_{\bar{x}\bar{x}}^{p}d\bar{z}+\int_{t_2}^{t_3}\frac{\partial\varphi\left(\bar{z}\right)}{\partial \bar{x}}\sigma_{\bar{x}\bar{x}}^{f}d\bar{z}\right)\\&M_{\bar{x}}=\int_{-h/2}^{h/2}\bar{z}\sigma_{\bar{x}\bar{x}}\left(\bar{z}\right)d\bar{z}=\left(\int_{t_0}^{t_1}\bar{z}\sigma_{\bar{x}\bar{x}}^{f}d\bar{z}+\int_{t_1}^{t_2}\bar{z}\sigma_{\bar{x}\bar{x}}^{p}d\bar{z}+\int_{t_2}^{t_3}\bar{z}\sigma_{\bar{x}\bar{x}}^{f}d\bar{z}\right)\\&M_{\bar{x}}=\int_{-h/2}^{h/2}\varphi\left(\bar{z}\right)\sigma_{\bar{x}\bar{x}}\left(\bar{z}\right)d\bar{z}=\\&\quad\left(\int_{t_0}^{t_1}\varphi\left(\bar{z}\right)\sigma_{\bar{x}\bar{x}}^{f}d\bar{z}+\int_{t_1}^{t_2}\varphi\left(\bar{z}\right)\sigma_{\bar{x}\bar{x}}^{p}d\bar{z}+\int_{t_2}^{t_3}\varphi\left(\bar{z}\right)\sigma_{\bar{x}\bar{x}}^{f}d\bar{z}\right)\end{aligned}\tag{21}$$

The integration constants presented in Eq. (20) can be presented as

$$\begin{aligned}&\bar{I}_A=\int_{-h/2}^{h/2}\rho\left(\bar{z}\right)d\bar{z}\\&\begin{Bmatrix}\bar{I}_{B1}\\\bar{I}_{B2}\end{Bmatrix}=\int_{-h/2}^{h/2}\begin{Bmatrix}\bar{z}\\\varphi\left(\bar{z}\right)\end{Bmatrix}\rho\left(\bar{z}\right)d\bar{z}\end{aligned}\tag{22}$$

$$\begin{Bmatrix} \bar{I}_{D1} \\ \bar{I}_{D2} \\ \bar{I}_{D3} \end{Bmatrix} = \int_{-h/2}^{h/2} \begin{Bmatrix} \bar{z}^2 \\ \bar{z}\varphi(\bar{z}) \\ \varphi(\bar{z})^2 \end{Bmatrix} \rho(\bar{z})\, d\bar{z}$$

In according to nonlocal strain gradient theory (Li and Hu 2016), the constitutive relations are expressed as

$$\begin{aligned} &\left(1-(\bar{e}_0\bar{a})^2\nabla^2\right)\sigma_{\bar{x}\bar{x}} = E(\bar{z})\left(1-\bar{l}_m^2\nabla^2\right)\varepsilon_{\bar{x}\bar{x}} - \\ &\qquad E(\bar{z})\alpha(\bar{z})\Delta T - e_{31}E_{\bar{z}} \\ &\left(1-(\bar{e}_0\bar{a})^2\nabla^2\right)\sigma_{\bar{x}\bar{z}} = G(z)\left(1-\bar{l}_m^2\nabla^2\right)\varepsilon_{\bar{x}\bar{z}} - e_{15}E_{\bar{x}} \\ &\left(1-(\bar{e}_0\bar{a})^2\nabla^2\right)D_{\bar{x}} = e_{15}\left(1-\bar{l}_m^2\nabla^2\right)\varepsilon_{\bar{x}\bar{z}} - k_{11}E_{\bar{x}} \\ &\left(1-(\bar{e}_0\bar{a})^2\nabla^2\right)D_{\bar{z}} = e_{31}\left(1-\bar{l}_m^2\nabla^2\right)\varepsilon_{\bar{x}\bar{x}} - k_{33}E_{\bar{z}} \end{aligned} \tag{23}$$

In Eq. (23), $\nabla^2 = \partial^2/\partial\bar{x}^2$ is the Laplacian operator, $\bar{e}_0\bar{a}$ is the nonlocal parameter and $\bar{l}_m$ is the strain gradient length scale parameter. The nonlocal strain gradient constitutive relations in Eq. (23) can be written as follows

$$\begin{aligned} &\sigma_{\bar{x}\bar{x}} - (\bar{e}_0\bar{a})^2\frac{\partial^2\sigma_{\bar{x}\bar{x}}}{\partial\bar{x}^2} = \left(1-\bar{l}_m^2\nabla^2\right)E(\bar{z})\times \\ &\quad\left[\frac{\partial u_0}{\partial\bar{x}} - \bar{z}\frac{\partial^2 w_0}{\partial\bar{x}^2} + \varphi\left(\frac{\partial^2 w_0}{\partial\bar{x}^2} - \frac{\partial\phi}{\partial\bar{z}}\right)\right] - E(\bar{z})\alpha(\bar{z})\Delta T - \\ &\quad e_{31}\left(\beta\sin(\beta\bar{z})\bar{\Phi}(\bar{x},\bar{t}) - E_0\right) \\ &\sigma_{\bar{x}\bar{z}} - (\bar{e}_0\bar{a})^2\frac{\partial^2\sigma_{\bar{x}\bar{z}}}{\partial\bar{x}^2} = \left(1-\bar{l}_m^2\nabla^2\right)G(\bar{z})\left[\frac{\partial\varphi}{\partial\bar{z}}\left(\frac{\partial w_0}{\partial\bar{x}} - \phi\right)\right] + \\ &\quad e_{15}\left(\cos(\beta\bar{z})\frac{\partial\bar{\Phi}}{\partial\bar{x}}\right) \\ &\left(1-(\bar{e}_0\bar{a})^2\nabla^2\right)D_{\bar{x}} = e_{15}\left(1-\bar{l}_m^2\nabla^2\right)\left[\frac{\partial\varphi}{\partial\bar{z}}\left(\frac{\partial w_0}{\partial\bar{x}} - \phi\right)\right] + \\ &\quad k_{11}\left(\cos(\beta\bar{z})\frac{\partial\bar{\Phi}}{\partial\bar{x}}\right) \\ &\left(1-(\bar{e}_0\bar{a})^2\nabla^2\right)D_{\bar{z}} = e_{31}\left(1-\bar{l}_m^2\nabla^2\right)\times \\ &\quad\left[\frac{\partial u_0}{\partial\bar{x}} - \bar{z}\frac{\partial^2 w_0}{\partial\bar{x}^2} + \varphi\left(\frac{\partial^2 w_0}{\partial\bar{x}^2} - \frac{\partial\phi}{\partial\bar{z}}\right)\right] - \\ &\quad k_{33}\left(\beta\sin(\beta\bar{z})\bar{\Phi}(\bar{x},\bar{t}) - E_0\right) \end{aligned} \tag{24}$$

Based on defined mechanical and electrical relations in Eq. (24), the resultant components can be calculated as follows

$$\begin{aligned} &N_{\bar{x}\bar{x}} - (\bar{e}_0\bar{a})^2\frac{\partial^2 N_{\bar{x}\bar{x}}}{\partial\bar{x}^2} = \left(1-\bar{l}_m^2\nabla^2\right)\times \\ &\quad\left[\bar{A}_{\bar{x}}\frac{\partial u_0}{\partial\bar{x}} - \bar{B}_{\bar{x}1}\frac{\partial^2 w_0}{\partial\bar{x}^2} + \bar{B}_{\bar{x}2}\left(\frac{\partial^2 w_0}{\partial\bar{x}^2} - \frac{\partial\phi}{\partial\bar{z}}\right)\right] - \bar{N}^T - \bar{N}^E \\ &M_{\bar{x}\bar{x}} - (\bar{e}_0\bar{a})^2\frac{\partial^2 M_{\bar{x}\bar{x}}}{\partial\bar{x}^2} = \left(1-\bar{l}_m^2\nabla^2\right)\times \\ &\quad\left[\bar{B}_{\bar{x}1}\frac{\partial u_0}{\partial\bar{x}} - \bar{D}_{\bar{x}1}\frac{\partial^2 w_0}{\partial\bar{x}^2} + \bar{D}_{\bar{x}2}\left(\frac{\partial^2 w_0}{\partial\bar{x}^2} - \frac{\partial\phi}{\partial\bar{z}}\right)\right] - \bar{M}^{T1} - \bar{M}^{E1} \\ &M^h_{\bar{x}\bar{x}} - (\bar{e}_0\bar{a})^2\frac{\partial^2 M^h_{\bar{x}\bar{x}}}{\partial\bar{x}^2} = \left(1-\bar{l}_m^2\nabla^2\right)\times \\ &\quad\left[\bar{B}_{\bar{x}2}\frac{\partial u_0}{\partial\bar{x}} - \bar{D}_{\bar{x}2}\frac{\partial^2 w_0}{\partial\bar{x}^2} + \bar{D}_{\bar{x}3}\left(\frac{\partial^2 w_0}{\partial\bar{x}^2} - \frac{\partial\phi}{\partial\bar{z}}\right)\right] - \bar{M}^{T2} - \bar{M}^{E2} \\ &Q_{\bar{x}\bar{z}} - (\bar{e}_0\bar{a})^2\frac{\partial^2 Q_{\bar{x}\bar{z}}}{\partial\bar{x}^2} = \left(1-\bar{l}_m^2\nabla^2\right)\bar{A}_{\bar{x}\bar{z}}\left[\frac{\partial w_0}{\partial\bar{x}} - \phi\right] + \\ &\quad\int_A e_{15}\left(\cos(\beta\bar{z})\frac{\partial\bar{\Phi}}{\partial\bar{x}}\right)dA \\ &\bar{D}_{\bar{x}} - (\bar{e}_0\bar{a})^2\frac{\partial^2\bar{D}_{\bar{x}}}{\partial\bar{x}^2} = \left(1-\bar{l}_m^2\nabla^2\right)e_{15}\frac{\partial\varphi}{\partial\bar{z}}\left[\frac{\partial w_0}{\partial\bar{x}} - \phi\right] - \\ &\quad k_{xx}\left(\cos(\beta\bar{z})\frac{\partial\bar{\Phi}}{\partial\bar{x}}\right) \\ &\bar{D}_{\bar{z}} - (\bar{e}_0\bar{a})^2\frac{\partial^2\bar{D}_{\bar{z}}}{\partial\bar{x}^2} = \left(1-\bar{l}_m^2\nabla^2\right)e_{31}\times \\ &\quad\left[\frac{\partial u_0}{\partial\bar{x}} - \bar{z}\frac{\partial^2 w_0}{\partial\bar{x}^2} + \varphi(\bar{z})\left(\frac{\partial w_0}{\partial\bar{x}} - \phi\right)\right] - \\ &\quad\alpha(\bar{z})\Delta T + k_{\bar{z}\bar{z}}\left(\beta\sin(\beta\bar{z})\bar{\Phi}(\bar{x},\bar{t}) - E_0\right) \end{aligned} \tag{25}$$

Where superscripts T and E represent thermal and electrical loads. Based on these comments, the force and moment resultants $\bar{N}^T$, $\bar{N}^E$, $\bar{M}^{T1}$, $\bar{M}^{T2}$, $\bar{M}^{E1}$ and $\bar{M}^{E2}$ are expressed as

$$\begin{aligned} &\begin{pmatrix} \bar{N}^T \\ \bar{N}^E \end{pmatrix} = \int_{-H/2}^{H/2}\begin{pmatrix} E(\bar{z})\alpha(\bar{z})\Delta T \\ -E_0 e_{31} \end{pmatrix} d\bar{z} \\ &\begin{pmatrix} \bar{M}^{T1} \\ \bar{M}^{E1} \end{pmatrix} = \int_{-H/2}^{H/2}\begin{pmatrix} E(\bar{z})\alpha(\bar{z})\Delta T \\ -E_0 e_{31} \end{pmatrix} \bar{z}\, d\bar{z} \\ &\begin{pmatrix} \bar{M}^{T2} \\ \bar{M}^{E2} \end{pmatrix} = \int_{-H/2}^{H/2}\begin{pmatrix} E(\bar{z})\alpha(\bar{z})\Delta T \\ -E_0 e_{31} \end{pmatrix} \varphi(\bar{z})\, d\bar{z} \end{aligned} \tag{26}$$

It is noted that, A_x, B_x and D_x in Eq. (25) are the stretching stiffness, stretching-bending coupling stiffness and bending stiffness coefficients, respectively, which can be obtained as

$$\begin{aligned} &\bar{A}_{\bar{x}} = \int_{-h/2}^{h/2} E(\bar{z})\, dA \\ &\begin{Bmatrix} \bar{B}_{\bar{x}1} \\ \bar{B}_{\bar{x}2} \end{Bmatrix} = \int_{-h/2}^{h/2}\begin{Bmatrix} \bar{z} \\ \varphi(\bar{z}) \end{Bmatrix} E(\bar{z})\, d\bar{z} \\ &\begin{Bmatrix} \bar{D}_{\bar{x}1} \\ \bar{D}_{\bar{x}2} \\ \bar{D}_{\bar{x}3} \end{Bmatrix} = \int_{-h/2}^{h/2}\begin{Bmatrix} \bar{z}^2 \\ \bar{z}\varphi(\bar{z}) \\ \varphi(\bar{z})^2 \end{Bmatrix} E(\bar{z})\, d\bar{z} \end{aligned} \tag{27}$$

To obtain the equations of motion, Eq. (25) should be substituted into Eq. (20). Therefore, four coupled equations of motion are obtained

$$\begin{aligned} &\delta u_0 : \left(1-l_m{}^2\nabla^2\right)\left(\bar{A}_{\bar{x}}\frac{\partial^2 u_0}{\partial\bar{x}^2} - \bar{B}_{\bar{x}1}\frac{\partial^3 w_0}{\partial\bar{x}^3} + \bar{B}_{\bar{x}2}\left(\frac{\partial^3 w_0}{\partial\bar{x}^3} - \frac{\partial^2\phi}{\partial\bar{z}^2}\right)\right) + \\ &\left(1-(\bar{e}_0\bar{a})^2\nabla^2\right)F = \\ &\left(1-(\bar{e}_0\bar{a})^2\nabla^2\right)\left(\bar{I}_A\frac{\partial^2 u_0}{\partial\bar{t}^2} - \bar{I}_{B1}\frac{\partial^3 w_0}{\partial\bar{t}^2\partial\bar{x}} + \bar{I}_{B2}\frac{\partial^3 w_0}{\partial\bar{t}^2\partial\bar{x}} - \bar{I}_{B2}\frac{\partial^2\phi}{\partial\bar{t}^2}\right) \end{aligned} \tag{28}$$

$$\delta w_0 : -\left(1-l_m{}^2\nabla^2\right)\left(\bar{B}_{\bar{x}2}\frac{\partial^2 u_0}{\partial \bar{x}^2}-\bar{D}_{\bar{x}2}\frac{\partial^4 w_0}{\partial \bar{x}^4}+\bar{D}_{\bar{x}3}\frac{\partial^4 w_0}{\partial \bar{x}^4}-\bar{D}_{\bar{x}3}\frac{\partial^3 \phi}{\partial \bar{x}^3}\right)$$
$$+\left(1-l_m{}^2\nabla^2\right)\left(-\bar{D}_{\bar{x}1}\frac{\partial^4 w_0}{\partial \bar{x}^4}+\bar{D}_{\bar{x}2}\frac{\partial^4 w_0}{\partial \bar{x}^4}-\bar{D}_{\bar{x}2}\frac{\partial^3 \phi}{\partial \bar{x}^3}\right)+\bar{M}^{E1}\frac{\partial^2 \bar{\Phi}}{\partial \bar{x}^2}-$$
$$\bar{M}^{E2}\frac{\partial^2 \bar{\Phi}}{\partial \bar{x}^2}-\bar{K}_w w_0+\bar{K}_s\frac{\partial^2 w_0}{\partial \bar{x}^2}+\bar{N}\frac{\partial^2 w_0}{\partial \bar{x}^2}+\bar{A}_{\bar{x}\bar{z}}\left(1-l_m{}^2\nabla^2\right)\frac{\partial^2 w_0}{\partial \bar{x}^2}$$
$$-\bar{A}_{\bar{x}\bar{z}}\left(1-l_m{}^2\nabla^2\right)\frac{\partial \phi}{\partial \bar{x}}+E^{15}\frac{\partial^2 \bar{\Phi}}{\partial \bar{x}^2}=\left(1-\left(\bar{e}_0\bar{a}\right)^2\nabla^2\right)\times$$
$$\left(\bar{I}_{B1}\frac{\partial^3 u_0}{\partial \bar{x}\partial \bar{t}^2}-\bar{I}_{B2}\frac{\partial^3 u_0}{\partial \bar{x}\partial \bar{t}^2}+\bar{I}_A\frac{\partial^2 w_0}{\partial \bar{t}^2}-\bar{I}_{D1}\frac{\partial^4 w_0}{\partial \bar{t}^2\partial \bar{x}^2}+\right.$$
$$\bar{I}_{D2}\frac{\partial^4 w_0}{\partial \bar{t}^2\partial \bar{x}^2}+\bar{I}_{D2}\frac{\partial^4 w_0}{\partial \bar{t}^2\partial \bar{x}^2}-\bar{I}_{D3}\frac{\partial^4 w_0}{\partial \bar{t}^2\partial \bar{x}^2}-\bar{I}_{D2}\frac{\partial^3 \phi}{\partial \bar{x}\partial \bar{t}^2}$$
$$\left.+\bar{I}_{D3}\frac{\partial^3 \phi}{\partial \bar{x}\partial \bar{t}^2}\right),\quad \bar{N}=\bar{N}_0-\left(\bar{N}^T-\bar{N}^E\right)$$

$$\delta\phi : \left(1-l_m{}^2\nabla^2\right)\bar{A}_{\bar{x}\bar{z}}\left(\frac{\partial w_0}{\partial \bar{x}}-\phi\right)+E^{15}\frac{\partial \bar{\Phi}}{\partial \bar{x}}-\left(1-l_m{}^2\nabla^2\right)\times$$
$$\left(\bar{B}_{\bar{x}2}\frac{\partial^2 u_0}{\partial \bar{x}^2}-\bar{D}_{\bar{x}2}\frac{\partial^3 w_0}{\partial \bar{x}^3}+\bar{D}_{\bar{x}3}\frac{\partial^3 w_0}{\partial \bar{x}^3}\right.$$
$$\left.-\bar{D}_{\bar{x}3}\frac{\partial^2 \phi}{\partial \bar{x}^2}\right)-E_3{}^{13}\frac{\partial \bar{\Phi}}{\partial \bar{x}}=\left(1-\left(\bar{e}_0\bar{a}\right)^2\nabla^2\right)\times$$
$$\left(\bar{I}_{B2}\frac{\partial^2 u_0}{\partial \bar{t}^2}+\bar{I}_{D2}\frac{\partial^3 w_0}{\partial \bar{t}^2\partial \bar{x}}-\bar{I}_{D3}\frac{\partial^3 w_0}{\partial \bar{t}^2\partial \bar{x}}+\bar{I}_{D3}\frac{\partial^2 \phi}{\partial \bar{t}^2}\right)$$
$$\delta\bar{\Phi} : \left(1-l_m{}^2\nabla^2\right)\left(E^{15}+E_3{}^{13}\right)\left(\frac{\partial^2 w_0}{\partial \bar{x}^2}-\frac{\partial \phi}{\partial \bar{x}}\right)-\left(1-l_m{}^2\nabla^2\right)\times$$
$$E_2^{31}\frac{\partial^2 w_0}{\partial \bar{x}^2}-k_{xx}\frac{\partial^2 \bar{\Phi}}{\partial \bar{x}^2}+k_{zz}\bar{\Phi}=0$$

In which, E^{15}, E_2^{31}, E_3^{31}, $k_{\bar{x}\bar{x}}$ and $k_{\bar{z}\bar{z}}$ are calculated as the following form

$$\begin{aligned}
E^{15} &= \int_A e_{15}\frac{\partial \varphi(\bar{z})}{\partial \bar{z}}\cos\left(\beta\bar{z}\right)dA\\
E_2^{31} &= \int_A \beta e_{31}\bar{z}\sin\left(\beta\bar{z}\right)dA\\
E_2^{31} &= \int_A \beta e_{31}\varphi(\bar{z})\sin\left(\beta\bar{z}\right)dA\\
k_{\bar{x}\bar{x}} &= \int_A k_{11}\cos^2\left(\beta\bar{z}\right)dA\\
k_{\bar{z}\bar{z}} &= \int_A k_{33}\beta^2\cos^2\left(\beta\bar{z}\right)dA
\end{aligned}\tag{29}$$

Also, all of the coefficients defined in Eq. (28) are presented in appendix A of this paper. By defining following non-dimensional variables as

$$\begin{aligned}
&x=\frac{\bar{x}}{L},\quad w=\frac{w_0}{h},\quad ,\mu_1=\frac{\bar{l}_m}{L},\quad \mu_2=\frac{\bar{e}_0\bar{a}}{L},\quad t=\frac{\bar{t}}{T_0},\\
&T_0=L\sqrt{\frac{\bar{I}_A}{\bar{A}_{\bar{x}}}},\quad R=\frac{h}{L},\quad A_{xz}=\frac{\bar{A}_{\bar{x}\bar{z}}}{\bar{A}_{\bar{x}}},\\
&\{I_{D1},I_{D2},I_{D3}\}=\frac{\{\bar{I}_{D1},\bar{I}_{D2},\bar{I}_{D3}\}}{\bar{I}_A L^2},\\
&\{D_{x1},D_{x2},D_{x3}\}=\frac{\{\bar{D}_{\bar{x}1},\bar{D}_{\bar{x}2},\bar{D}_{\bar{x}3}\}}{\bar{A}_{\bar{x}}L^2},\\
&N^T=\frac{\bar{N}^T}{\bar{A}_{\bar{x}}},\quad N^E=\frac{\bar{N}^E}{\bar{A}_{\bar{x}}},\quad M^{E1}=\frac{\bar{M}^{E1}\Phi_0}{\bar{A}_{\bar{x}}h},\\
&M^{E2}=\frac{\bar{M}^{E2}\Phi_0}{\bar{A}_{\bar{x}}h},\quad \Phi_0=\frac{\bar{A}_x}{e_{15}},\quad \Phi=\frac{\tilde{\Phi}}{\Phi_0}\\
&E^{15}=\frac{\bar{E}^{15}\Phi_0}{\bar{A}_{\bar{x}}h},\qquad E_{2\ and\ 3}^{31}=\frac{\bar{E}_{2\,and\,3}^{31}\Phi_0}{\bar{A}_{\bar{x}}h},\\
&K_w=\frac{\bar{K}_w L^2}{\bar{A}_{\bar{x}}},\qquad K_s=\frac{\bar{K}_s}{\bar{A}_{\bar{x}}},\qquad k_{xx}=\frac{\bar{k}_{\bar{x}\bar{x}}\Phi_0^2}{\bar{A}_{\bar{x}}h^2},\\
&k_{zz}=\frac{\bar{k}_{\bar{z}\bar{z}}\Phi_0^2}{\bar{A}_{\bar{x}}}
\end{aligned}\tag{30}$$

The final dimensionless equations of motion are obtained as

$$\begin{aligned}
&\delta u : \left(1-\mu_1{}^2\nabla^2\right)\left(\frac{\partial^2 u}{\partial x^2}+\frac{\partial w_0}{\partial x}\frac{\partial^2 w_0}{\partial x^2}\right)+\left(1-\mu_2{}^2\nabla^2\right)F=\\
&\left(1-\mu_2{}^2\nabla^2\right)\frac{\partial^2 u}{\partial t^2}\\
&\delta w_0 : -\left(1-l_m{}^2\nabla^2\right)\left(B_{x2}\frac{\partial^2 u}{\partial x^2}-D_{x2}\frac{\partial^4 w}{\partial x^4}+D_{x3}\frac{\partial^4 w}{\partial x^4}-D_{x3}\frac{\partial^3 \phi}{\partial x^3}\right)\\
&+\left(1-l_m{}^2\nabla^2\right)\left(-D_{x1}\frac{\partial^4 w}{\partial x^4}+D_{x2}\frac{\partial^4 w}{\partial x^4}-D_{x2}\frac{\partial^3 \phi}{\partial x^3}\right)+\\
&M^{E1}\frac{\partial^2 \Phi}{\partial x^2}-M^{E2}\frac{\partial^2 \Phi}{\partial x^2}-K_w w+K_s\frac{\partial^2 w}{\partial x^2}+N\frac{\partial^2 w_0}{\partial x^2}+\\
&A_{xz}\left(1-l_m{}^2\nabla^2\right)\frac{\partial^2 w}{\partial x^2}-A_{xz}\left(1-l_m{}^2\nabla^2\right)\frac{\partial \phi}{\partial x}+E^{15}\frac{\partial^2 \Phi}{\partial x^2}\\
&=\left(1-\left(e_0 a\right)^2\nabla^2\right)\left(I_{B1}\frac{\partial^3 u}{\partial x\partial t^2}-I_{B2}\frac{\partial^3 u}{\partial x\partial t^2}+I_A\frac{\partial^2 w}{\partial t^2}\right.\\
&-I_{D1}\frac{\partial^4 w}{\partial t^2\partial x^2}+I_{D2}\frac{\partial^4 w}{\partial t^2\partial x^2}+I_{D2}\frac{\partial^4 w}{\partial t^2\partial x^2}-I_{D3}\frac{\partial^4 w}{\partial t^2\partial x^2}\\
&\left.-I_{D2}\frac{\partial^3 \phi}{\partial x\partial t^2}+I_{D3}\frac{\partial^3 \phi}{\partial x\partial t^2}\right)\\
&\delta\phi : \left(1-\mu_1{}^2\nabla^2\right)A_{xz}\left(\frac{\partial w}{\partial x}-\phi\right)+E^{15}\frac{\partial \Phi}{\partial x}-\left(1-\mu_1{}^2\nabla^2\right)\times\\
&\left(-D_{x2}\frac{\partial^3 w}{\partial x^3}+D_{x3}\frac{\partial^3 w}{\partial x^3}-D_{x3}\frac{1}{R}\frac{\partial^2 \phi}{\partial x^2}\right)-\\
&E_3{}^{13}\frac{\partial \Phi}{\partial x}=\left(1-\mu_2{}^2\nabla^2\right)\left(I_{D2}\frac{\partial^3 w}{\partial t^2\partial x}-I_{D3}\frac{\partial^3 w}{\partial t^2\partial x}+I_{D3}\frac{\partial^2 \phi}{\partial t^2}\right)\\
&\delta\Phi : \left(1-\mu_1{}^2\nabla^2\right)\left(E^{15}+E_3{}^{13}\right)\left(\frac{\partial^2 w}{\partial x^2}-\frac{1}{R}\frac{\partial \phi}{\partial x}\right)-\\
&\left(1-\mu_1{}^2\nabla^2\right)E_2^{31}\frac{\partial^2 w}{\partial x^2}-k_{xx}\frac{\partial^2 \Phi}{\partial x^2}+k_{zz}\frac{1}{R^2}\Phi=0
\end{aligned}\tag{31}$$

Boundary conditions to solve Eq. (31) are defined as (Ansari *et al.* 2014)

$$\begin{aligned}
&u=w=\phi=\Phi=0 \qquad \textit{for clamped ends}\\
&u=w=\frac{\partial\phi}{\partial x}=\Phi=0 \qquad \textit{for hinged ends}
\end{aligned}\tag{32}$$

4. Buckling analysis

In order to solve the linear governing equations of motion for obtaining the critical thermal, mechanical and electrical loads, DQ method is employed. Based on the aforementioned method, the approximate solution of a function $f(x)$ can be found in the form

$$f(x)=\sum_{j=1}^{N}\lambda_j\psi_j(x) \tag{33}$$

Where, N is the total number of grid points inside a closed interval. In this method, the smooth basis functions are selected as the various functions form such as Chebyshev polynomials, Exponential polynomials, and Fourier polynomials (Tornabene *et al.* 2014, Tornabene *et al.* 2014). Also, the Eq. (33) for the one-dimensional case can be written in matrix form as

$$\boldsymbol{f}=\boldsymbol{C\lambda} \tag{34}$$

In which, $\boldsymbol{f}=[f(x_1),f(x_2),f(x_3),\dots,f(x_N)]^T$ is the vector of the unknown function values, $\boldsymbol{\lambda}$ is the vector of the unknown coefficients λ_j and the components of the coefficient matrix $\boldsymbol{C}$ are given by $C_{ij}=\psi_j(x_i)$ for $i,j=1.2.3,\dots,N$ (Tornabene, Fantuzzi *et al.* 2014). Since the n'th order derivative of the Eq. (33) can be computed, the derivative is directly transferred to the functions $\psi_j(x)$, because the unknown coefficients λ_j do not depend on the variable x (Tornabene *et al.* 2014)

$$\frac{d^n f(x)}{dx^n}=\sum_{j=1}^{N}\lambda_j\frac{d^n\psi_j(x)}{dx^n},\quad for\quad n=1,2,3,\dots\dots,N-1 \tag{35}$$

Eq. (35) is rewritten as following matrix form

$$f^{(n)}=C^{(n)}\lambda\ \ with\ \ C_{ij}^{(n)}=\left.\frac{d^n\psi_j(x)}{dx^n}\right|_{x_i}=\psi_j^{(n)}(x)$$
$$for\ \ i,j=1,2,3,\dots,N \tag{36}$$

Therefore, the governing equations and boundary conditions are discretized by means of aforementioned method (Ghorbanpour Arani *et al.* 2012, Ghorbanpour Arani *et al.* 2012). In this investigation, the cosine pattern is employed to generate the DQ point system as the following form

$$x_j=\frac{1}{2}\left\{1-\cos\left(\frac{\pi(j-1)}{N-1}\right)\right\},\qquad j=1,2,\dots\dots,N \tag{37}$$

In addition, column vectors for variables u, w, ϕ and Φ are considered as follows

$$u=[u_1\ \ u_2\ \ \dots\ \ u_N],\quad w=[w_1\ \ w_2\ \ \dots\ \ w_N],$$
$$\phi=[\phi_1\ \ \phi_2\ \ \dots\ \ \phi_N],\quad \Phi=[\Phi_1\ \ \Phi_2\ \ \dots\ \ \Phi_N], \tag{38}$$

To solve Eq. (31) and associated boundary conditions Eq. (32) for nonlinear vibration analysis of the sandwich nano-beam by DQ method, the weighting coefficients for the second, third and fourth derivatives with attention to Eq. (36) are determined as the following form

$$\left.\frac{\partial^r f(\varsigma,\lambda)}{\partial\varsigma^r}\right|_{(\varsigma,\lambda)=(\varsigma_j,\lambda_j)}=\sum_{j=1}^{N_\varsigma}C_{ij}^{\varsigma(r)}f(\varsigma_j,\lambda_m)=$$
$$\sum_{j=1}^{N_\varsigma}C_{ij}^{\varsigma(r)}f_{jm},\begin{cases}i=1,2,\dots,N_\varsigma\\ m=1,2,\dots,N_\lambda\\ r=1,2,\dots,N_\varsigma-1\end{cases} \tag{39}$$

In which weighting coefficients C_{ij}^{ζ} are expressed as

$$\left.\frac{\partial^r f(\varsigma,\lambda)}{\partial\varsigma^r}\right|_{(\varsigma,\lambda)=(\varsigma_j,\lambda_j)}=\sum_{j=1}^{N_\varsigma}C_{ij}^{\varsigma(r)}f(\varsigma_j,\lambda_m)=$$
$$\sum_{j=1}^{N_\varsigma}C_{ij}^{\varsigma(r)}f_{jm},\begin{cases}i=1,2,\dots,N_\varsigma\\ m=1,2,\dots,N_\lambda\\ r=1,2,\dots,N_\varsigma-1\end{cases}$$
$$C_{ij}^{\varsigma}=\begin{cases}\dfrac{M(\varsigma_i)}{(\varsigma_i-\varsigma_j)M(\varsigma_j)} & for\quad i\neq j\\ -\displaystyle\sum_{\substack{j=1\\ i\neq j}}^{N_\varsigma}C_{ij}^{\varsigma} & for\quad i=j\end{cases} \tag{40}$$

It is noted that in Eq. (40), $M(\varsigma_i)$ is represented as following form

$$M(\varsigma_i)=\prod_{\substack{j=1\\ i\neq j}}^{N_\varsigma}(\varsigma_i-\varsigma_j) \tag{41}$$

The weighting coefficients for various derivatives such as the second, third and fourth derivatives are defined as

$$M(\varsigma_i)=\prod_{\substack{j=1\\ i\neq j}}^{N_\varsigma}(\varsigma_i-\varsigma_j)$$
$$C_{ij}^{\varsigma(2)}=\sum_{k=1}^{N\varsigma}C_{ik}^{\varsigma(1)}C_{kj}^{\varsigma(1)},$$
$$C_{ij}^{\varsigma(3)}=\sum_{k=1}^{N\varsigma}C_{ik}^{\varsigma(1)}C_{kj}^{\varsigma(2)}=\sum_{k=1}^{N\varsigma}C_{ik}^{\varsigma(2)}C_{kj}^{\varsigma(1)},$$
$$C_{ij}^{\varsigma(4)}=\sum_{k=1}^{N\varsigma}C_{ik}^{\varsigma(1)}C_{kj}^{\varsigma(3)}=\sum_{k=1}^{N\varsigma}C_{ik}^{\varsigma(3)}C_{kj}^{\varsigma(1)} \tag{42}$$

Applying Eqs. (39) and (40) to Eq. (31) and also setting the inertia terms to zero and $N_0=-P$, one can obtain a set of differential equations as

$$\delta u:\sum_{m=1}^{N}C_{im}^{(2)}u_m+R\sum_{m=1}^{N}C_{im}^{(1)}w_m\sum_{m=1}^{N}C_{im}^{(2)}w_m-$$
$$\mu_1^2\left(\sum_{m=1}^{N}C_{im}^{(4)}u_m+3R\sum_{m=1}^{N}C_{im}^{(2)}w_m\sum_{m=1}^{N}C_{im}^{(3)}w_m\right.$$
$$\left.+R\sum_{m=1}^{N}C_{im}^{(1)}w_m\sum_{m=1}^{N}C_{im}^{(4)}w_m\right)=0$$
$$\delta w:\left(D_{x2}\sum_{m=1}^{N}C_{im}^{(4)}w_m-D_{x3}\sum_{m=1}^{N}C_{im}^{(4)}w_m+D_{x3}\frac{1}{R}\sum_{m=1}^{N}C_{im}^{(3)}\phi_m\right)+$$
$$\mu_1^2\left(-D_{x2}\sum_{m=1}^{N}C_{im}^{(6)}w_m+D_{x3}\sum_{m=1}^{N}C_{im}^{(6)}w_m-D_{x3}\frac{1}{R}\sum_{m=1}^{N}C_{im}^{(5)}\phi_m\right)$$
$$+\left(-D_{x1}\sum_{m=1}^{N}C_{im}^{(4)}w_m+D_{x2}\sum_{m=1}^{N}C_{im}^{(4)}w_m-D_{x2}\frac{1}{R}\sum_{m=1}^{N}C_{im}^{(3)}\phi_m\right)+$$
$$\mu_1^2\left(+D_{x1}\sum_{m=1}^{N}C_{im}^{(6)}w_m-D_{x2}\sum_{m=1}^{N}C_{im}^{(6)}w_m+D_{x2}\frac{1}{R}\sum_{m=1}^{N}C_{im}^{(5)}\phi_m\right)$$
$$-P\sum_{m=1}^{N}C_{im}^{(2)}w_m+M^{E1}\sum_{m=1}^{N}C_{im}^{(2)}\Phi_m-M^{E2}\sum_{m=1}^{N}C_{im}^{(2)}\Phi_m+$$
$$N\sum_{m=1}^{N}C_{im}^{(2)}w_m-K_w w_m+K_s\sum_{m=1}^{N}C_{im}^{(2)}w_m-K_{nl}w_m^3+A_{xz}\sum_{m=1}^{N}C_{im}^{(2)}w_m$$
$$-A_{xz}\mu_1^2\sum_{m=1}^{N}C_{im}^{(2)}w_m-A_{xz}\frac{1}{R}\sum_{m=1}^{N}C_{im}^{(1)}w_m+A_{xz}\frac{\mu_1^2}{R}\sum_{m=1}^{N}C_{im}^{(3)}w_m$$
$$+E^{15}\sum_{m=1}^{N}C_{im}^{(2)}\Phi_m=0 \tag{43}$$

$$\delta\phi: A_{xz}\left(\sum_{m=1}^{N} C_{im}^{(1)} w_m - \phi_m\right) - \mu_1^{2}\left(\sum_{m=1}^{N} C_{im}^{(3)} w_m - \sum_{m=1}^{N} C_{im}^{(3)} \phi_m\right) +$$
$$E^{15}\sum_{m=1}^{N} C_{im}^{(1)} \Phi_m + \Bigg(D_{x2}\sum_{m=1}^{N} C_{im}^{(3)} w_m - D_{x3}\sum_{m=1}^{N} C_{im}^{(3)} w_m +$$
$$D_{x3}\frac{1}{R}\sum_{m=1}^{N} C_{im}^{(2)} \phi_m - E_3^{13}\sum_{m=1}^{N} C_{im}^{(1)} \Phi_m + \mu_1^{2}\Bigg(-D_{x2}\sum_{m=1}^{N} C_{im}^{(5)} w_m +$$
$$D_{x3}\sum_{m=1}^{N} C_{im}^{(5)} w_m - D_{x3}\frac{1}{R}\sum_{m=1}^{N} C_{im}^{(4)} \phi_m = 0$$

$$\delta\Phi: E^{15}\sum_{m=1}^{N} C_{im}^{(2)} w_m - E^{15}\frac{1}{R}\sum_{m=1}^{N} C_{im}^{(1)} \phi_m - \mu_1^{2}E^{15}\sum_{m=1}^{N} C_{im}^{(4)} w_m +$$
$$\mu_1^{2}E^{15}\frac{1}{R}\sum_{m=1}^{N} C_{im}^{(3)} \phi_m + E_3^{13}\sum_{m=1}^{N} C_{im}^{(2)} w_m - E_3^{13}\frac{1}{R}\sum_{m=1}^{N} C_{im}^{(1)} \phi_m -$$
$$\mu_1^{2}E_3^{13}\sum_{m=1}^{N} C_{im}^{(4)} w_m + \mu_1^{2}E_3^{13}\frac{1}{R}\sum_{m=1}^{N} C_{im}^{(3)} \phi_m - E_2^{31}\sum_{m=1}^{N} C_{im}^{(2)} w_m +$$
$$\mu_1^{2}E_2^{31}\sum_{m=1}^{N} C_{im}^{(4)} w_m - k_{xx}\sum_{m=1}^{N} C_{im}^{(4)} \Phi_m + k_{zz}\frac{1}{R^2}\Phi_m = 0$$

The boundary conditions of the sandwich nano-beam using DQ method are expressed as

$$\begin{cases} u_1 = w_1 = \phi_1 = \Phi_1 = 0 \\ u_N = w_N = \phi_N = \Phi_N = 0 \end{cases} \qquad \textit{for clamped ends}$$

$$\begin{cases} u_1 = w_1 = \sum_{m=1}^{N} C_{1m}^{(1)} \phi_m = \Phi_1 = 0 \\ u_N = w_N = \sum_{m=1}^{N} C_{Nm}^{(1)} \phi_m = \Phi_N = 0 \end{cases} \qquad \textit{for hinged ends} \tag{44}$$

After implementation of the boundary conditions, Eq. (43) can be written in matrix form as

$$\left([S] - P[A]\right)\{U_d\} = \{0\} \tag{45}$$

Clearly, the lowest positive solution of Eq. (45) gives the critical buckling load P_{cr}.

5. Numerical results and discussion

In this section, a parametric study is implemented to indicate the influences various HSDBTs, length scale parameter (strain gradient parameter), nonlocal parameter, volume fraction of the CNTs, parameters of Pasternak's foundation, various boundary conditions, the CNTs efficiency parameter, geometric dimensions and other important parameters on designing and controlling the buckling behaviors of sandwich nano-beam with FG-CNTRC face-sheets. The material properties and geometrical specifications of the sandwich nano-beam are presented in Table 1.

5.1 Comparison and validation

To justify the accuracy and trueness of the governing equations extracted in this study, a comparison with existing reference is represented. Fig. 3 shows comparison between the obtained results by solving the governing equations

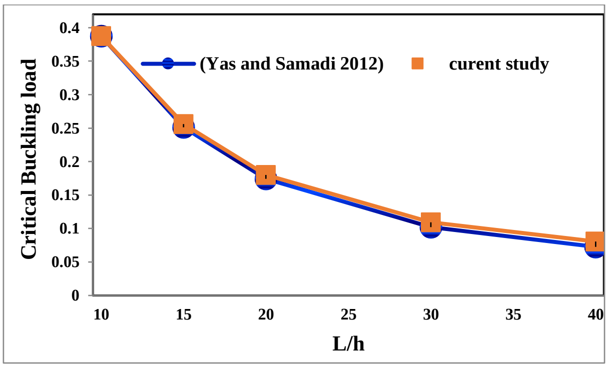

Fig. 2 critical buckling load versus length to height ratio (L/h)

Table 1 The material and geometrical properties of the constituent material of the FG nano-beam (Ke *et al.* 2010, Rafiee *et al.* 2013)

materials	Young's moduli (GP)	Heat expansion coefficient $(1/C^{o})$	$e_{31}(C/m^2)$	$e_{15}(C/m^2)$	$k_{11}(C/Vm)$	$k_{33}(C/Vm)$
piezoelectric	226	0.9×10^{-6}	-2.2	5.8	5.64×10^{-9}	6.35×10^{-9}
CNT	5.6×10^{3}	3.4584×10^{-6}				

Table 2 The Mechanical Critical load for different HOSDBTs with varying nonlocal parameter

	C_S Boundary Condition					
	FSDBT	PSDBT	TSDBT	HSDBT	ESDBT	ASDBT
e_0a	N_m^{cr}					
0.02	2.2676	2.2546	2.2550	2.2711	2.2543	2.2543
0.04	2.2146	2.2021	2.2024	2.2250	2.2018	2.2018
0.06	2.1317	2.1198	2.1201	2.1441	2.1195	2.1195
0.08	2.0255	2.0144	2.0147	2.0381	2.0142	2.0142
0.10	1.9035	1.8935	1.8937	1.9160	1.8933	1.8933
0.12	1.7731	1.7640	1.7642	1.7863	1.7639	1.7638
0.14	1.6403	1.6322	1.6323	1.6470	1.6321	1.6321
0.16	1.5099	1.5028	1.5028	1.5202	1.5027	1.5026
0.18	1.3852	1.3789	1.3790	1.4554	1.3790	1.3790
0.20	1.2681	1.2621	1.2623	1.2862	1.2621	1.2618

Table 3 The Critical voltage for different HOSDBTs with varying nonlocal parameter

	C_S Boundary Condition					
	FSDBT	PSDBT	TSDBT	HSDBT	ESDBT	ASDBT
e_0a	$V_0^{cr}(mV)$					
0.02	276.53	274.95	275.00	276.96	274.91	274.91
0.04	270.07	268.55	268.59	271.34	268.51	268.51
0.06	259.96	258.51	258.55	261.48	258.48	258.48
0.08	247.01	245.66	245.70	248.55	245.64	245.63
0.10	232.14	230.91	230.94	233.66	230.89	230.88
0.12	216.23	215.12	215.14	217.84	215.11	215.10
0.14	200.04	199.04	199.06	200.85	199.04	199.03
0.16	184.14	183.27	183.27	185.39	183.25	183.25
0.18	168.93	168.16	168.17	177.49	168.17	168.17

Table 4 The Critical temperature rising for different HOSDBTs with varying nonlocal parameter

C_S Boundary Condition						
	FSDBT	PSDBT	TSDBT	HSDBT	ESDBT	ASDBT
e_0a	$\Delta T^{cr}(\dot{C})$					
0.02	1890	1879	1879	1893	1879	1879
0.04	1846	1835	1835	1854	1835	1835
0.06	1776	1767	1767	1787	1766	1766
0.08	1688	1679	1679	1698	1679	1679
0.10	1586	1578	1578	1597	1578	1578
0.12	1478	1470	1470	1489	1470	1470
0.14	1367	1360	1360	1372	1360	1360
0.16	1258	1252	1252	1267	1252	1252
0.18	1154	1149	1149	1213	1149	1149
0.20	1057	1052	1052	1072	1052	1051

Table 5 The Mechanical Critical load for different HOSDBTs with varying nonlocal parameter

C_C Boundary Condition						
	FSDBT	PSDBT	TSDBT	HSDBT	ESDBT	ASDBT
e_0a	N_m^{cr}					
0.02	4.3970	4.3540	4.3550	4.4470	4.3529	4.3529
0.04	4.2029	4.1625	4.1635	4.2446	4.1617	4.1617
0.06	3.9148	3.8785	3.8792	3.9523	3.8778	3.8778
0.08	3.5723	3.5405	3.5410	3.6037	3.5400	3.5400
0.10	3.2115	3.1843	3.1845	3.2342	3.1840	3.1840
0.12	2.8594	2.8368	2.8368	2.8685	2.8367	2.8367
0.14	2.5329	2.5168	2.5164	2.5126	2.5173	2.5172
0.16	2.2427	2.2079	2.2247	2.1539	2.1940	2.1940
0.18	1.9963	1.7355	1.7489	1.7335	1.7243	1.7243
0.20	1.6102	1.4007	1.4116	1.4097	1.3916	1.3916
S_S Boundary Condition						
	FSDBT	PSDBT	TSDBT	HSDBT	ESDBT	ASDBT
e_0a	N_m^{cr}					
0.02	1.1155	1.1131	1.1131	1.1220	1.1131	1.1131
0.04	1.1025	1.1001	1.1001	1.1095	1.1002	1.1001
0.06	1.0815	1.0791	1.0791	1.0881	1.0792	1.0792
0.08	1.0534	1.0511	1.0511	1.0582	1.0511	1.0511
0.10	1.0193	1.0171	1.0171	1.0246	1.0171	1.0171
0.12	0.9805	0.9784	0.9784	0.9878	0.9785	0.9785
0.14	0.9384	0.9364	0.9363	0.9416	0.9364	0.9364
0.16	0.8940	0.8921	0.8921	0.8978	0.8921	0.8921
0.18	0.8485	0.8467	0.8467	0.8498	0.8467	0.8467
0.20	0.8029	0.8012	0.8012	0.8026	0.8012	0.8012

extracted in this study and equation of motion obtained in Ref. (Yas and Samadi 2012). It is worthy noted that the Winkler and Pasternak foundation parameter effects were considered in Ref. (Yas and Samadi 2012). According to this comparison it is deduced that the present results are in a good agreement with the obtained results by Ref. (Yas and Samadi 2012). One can conclude that buckling load is decreased with increase of ratio L/h.

Table 6 the Mechanical Critical load, Critical voltage and Critical temperature rising for different HOSDBTs with varying small scale parameter (strain gradient parameter)

S_S Boundary Condition						
	FSDBT	PSDBT	TSDBT	HSDBT	ESDBT	ASDBT
l_m	N_m^{cr}					
0.002	1.1111	1.1087	1.1087	1.1175	1.1088	1.1088
0.004	1.1113	1.1089	1.1089	1.1176	1.1089	1.1089
0.006	1.1115	1.1091	1.1091	1.1179	1.1091	1.1091
0.008	1.1118	1.1094	1.1094	1.1182	1.1094	1.1094
0.010	1.1122	1.1098	1.1098	1.1186	1.1098	1.1098
0.012	1.1127	1.1103	1.1103	1.1190	1.1103	1.1103
0.014	1.1133	1.1108	1.1108	1.1196	1.1109	1.1109
0.016	1.1139	1.1115	1.1115	1.1203	1.1115	1.1115
0.018	1.1147	1.1122	1.1122	1.1210	1.1123	1.1123
0.020	1.1155	1.1131	1.1131	1.1220	1.1131	1.1131
S_S Boundary Condition						
	FSDBT	PSDBT	TSDBT	HSDBT	ESDBT	ASDBT
l_m	$V_0^{cr}(mv)$					
0.002	135.5057	135.213	135.21	136.2804	135.2176	135.2176
0.004	135.5218	135.229	135.226	136.2965	135.2337	135.2337
0.006	135.5485	135.2557	135.2527	136.3234	135.2603	135.2603
0.008	135.5859	135.2931	135.2901	136.3611	135.2977	135.2977
0.010	135.6341	135.3411	135.3381	136.4094	135.3458	135.3458
0.012	135.6929	135.3998	135.3968	136.4689	135.4045	135.4045
0.014	135.7625	135.4692	135.4662	136.5376	135.4739	135.4739
0.016	135.8427	135.5493	135.5463	136.6254	135.5539	135.554
0.018	135.9336	135.6401	135.6372	136.7088	135.644	135.6441
0.020	136.0347	135.741	135.7381	136.8252	135.7466	135.7499
S_S Boundary Condition						
	FSDBT	PSDBT	TSDBT	HSDBT	ESDBT	ASDBT
l_m	$\Delta T^{cr}(\dot{C})$					
0.002	925.96	923.96	923.94	931.25	923.99	923.99
0.004	926.07	924.07	924.04	931.36	924.10	924.10
0.006	926.25	924.25	924.23	931.54	924.28	924.28
0.008	926.50	924.50	924.48	931.80	924.53	924.53
0.010	926.83	924.83	924.81	932.13	924.86	924.86
0.012	927.24	925.23	925.21	932.54	925.26	925.26
0.014	927.71	925.71	925.69	933.01	925.74	925.74
0.016	928.26	926.25	926.23	933.61	926.28	926.29
0.018	928.88	926.87	926.85	934.18	926.90	926.90
0.020	929.57	927.56	927.54	934.97	927.60	927.62

5.2 Parametric study

The Mechanical Critical loads of the sandwich nano-beam with FG-CNTRC face-sheets in term of different nonlocal parameter are calculated for various HOSDBTs in Table 3. According to these results, it can be concluded that increasing the nonlocal parameter leads to decrease the Mechanical Critical loads. It is because of aforementioned parameter causes decreasing the stiffness of the sandwich nano-beam. Other conclusion that can be deduced form the results represented in this table is the amounts of the Mechanical Critical load calculated by PSDBT and TSDBT approximately have same values as well as ESDBT and ASDBT. Also, it is worthy noted that buckling load calculated by aforementioned theories are smaller than buckling load estimated by FSDBT.

Furthermore, regard to the obtained results presented in Table 3, the Critical voltage of the sandwich nano-beam is decreased by increasing the nonlocal parameter. The obtained results indicated critical voltage calculated by HSDBT has bigger value rather than other HOSDBTs.

The Critical temperature rising in term of nonlocal parameter is presented in Table 3. According to these results increasing the nonlocal parameter caused decrease of the Critical temperature rising.

The Mechanical Critical load for two other boundary conditions (clamped-clamped and simple-simple) is calculated in Table 5.

In Table 6, the Mechanical Critical load, Critical voltage and Critical temperature rising for various small scale parameters (strain gradient parameter) are presented. According to these results can be deduced that increasing strain gradient parameter caused to increase of the Mechanical Critical load, Critical voltage and Critical temperature rising for the sandwich nano-beam with various HOSDBTs and different boundary conditions.

The influences of strain gradient parameter on Mechanical Critical load are investigated for various boundary conditions in Table 7. Regard to these results, it is concluded that increase of strain gradient parameter on buckling behavior is independent from boundary conditions.

The effects of CNTs distribution patterns in face-sheets with varying height to length ratio on buckling behavior are studied in Table 8. In accordance to these results it can be deduced that AV pattern has the smallest Mechanical Critical load, Critical voltage and Critical temperature rising with respect to other distribution patterns. Also increasing the height to length ratio caused to increase the Mechanical Critical load, Critical voltage and Critical temperature rising.

In accordance to results presented in Table 9, it can be deduced that enhancing the volume fraction of CNTs in face-sheets and efficiency parameter lead to increase of the Mechanical Critical load. In addition, if Mechanical Critical load and electrical load are simultaneously applied on sandwich nano-beam, the increase of electrical load leads to decrease the buckling mechanical load.

In order to investigate the effects of Winkler parameter of elastic foundation on non-linear buckling behavior of the sandwich nano-beams, Mechanical Critical loads are calculated in Table 10 for three different thermal loads with varying Winkler parameter foundation. Regard to the results, it is noted that with increasing the Winkler foundation, the Mechanical Critical load increases. In addition, the Mechanical Critical load decreases by enhancing simultaneously thermal load.

The influences of the $\frac{h_f}{h_H}$ ratio and Pasternak coefficient of elastic foundation on Mechanical Critical load are studied in Table 11. Regarding to aforementioned results can be concluded that enhancing the $\frac{h_f}{h_H}$ ratio and Pasternak coefficient lead to increase of the Mechanical Critical load in whole of the volume fraction of CNTs in face-sheets and efficiency parameter.

The effects of the considering different small scale theories on buckling behavior of the sandwich nano-beam are presented in Table 12. According to these results, nonlocal elasticity theory (NET) has the smallest Mechanical Critical loads with respect to other theories such as nonlocal strain gradient elasticity theory (NSGET) and classic elasticity theory (CET) in various HOSDBTs.

Table 7 The Mechanical Critical load for different HOSDBTs with varying small scale parameter (strain gradient parameter)

S_C Boundary Condition						
	FSDBT	PSDBT	TSDBT	HSDBT	ESDBT	ASDBT
l_m	N_m^{cr}					
0.002	2.2499	2.2376	2.2378	2.2696	2.2374	2.2374
0.004	2.2504	2.2381	2.2383	2.2701	2.2379	2.2379
0.006	2.2513	2.2390	2.2392	2.2708	2.2388	2.2388
0.008	2.2526	2.2402	2.2405	2.2718	2.2400	2.2400
0.010	2.2542	2.2418	2.2420	2.2730	2.2415	2.2415
0.012	2.2562	2.2437	2.2440	2.2744	2.2434	2.2434
0.014	2.2585	2.2459	2.2462	2.2758	2.2457	2.2457
0.016	2.2612	2.2485	2.2488	2.2769	2.2482	2.2482
0.018	2.2642	2.2514	2.2517	2.2796	2.2511	2.2511
0.020	2.2676	2.2546	2.2550	0.4677	2.2543	2.2543
C_C Boundary Condition						
	FSDBT	PSDBT	TSDBT	HSDBT	ESDBT	ASDBT
l_m	N_m^{cr}					
0.002	4.3306	4.2907	4.2912	4.4107	4.2903	4.2903
0.004	4.3327	4.2927	4.2932	4.4124	4.2922	4.2922
0.006	4.3360	4.2959	4.2965	4.4151	4.2955	4.2955
0.008	4.3408	4.3005	4.3011	4.4188	4.3000	4.3000
0.010	4.3469	4.3064	4.3070	4.4234	4.3058	4.3058
0.012	4.3543	4.3135	4.3142	4.4287	4.3129	4.3129
0.014	4.3631	4.3219	4.3226	4.4343	4.3212	4.3212
0.016	4.3731	4.3314	4.3323	4.4394	4.3307	4.3307
0.018	4.3845	4.3422	4.3431	4.4428	4.3413	4.3413
0.020	4.3970	4.3540	4.3550	0.3970	4.3529	4.3529

6. Conclusions

Table 8 the Mechanical Critical load, Critical voltage and Critical temperature rising for different CNTs distribution patterns in face-sheets with varying height to length ratio

	ASDBT & S_S Boundary Condition			HSDBT & S_S Boundary Condition			FSDBT & S_S Boundary Condition		
	AV	UU	VA	AV	UU	VA	AV	UU	VA
$R=\frac{h}{L}$		N_m^{cr}			N_m^{cr}			N_m^{cr}	
0.0385	0.7227	1.3675	0.9494	0.7265	1.3772	0.9588	0.9512	1.3702	1.2539
0.0357	0.6235	1.1800	0.8193	0.6258	1.1854	0.8244	0.8206	1.1820	1.0788
0.0333	0.5434	1.0286	0.7142	0.5453	1.0357	0.7172	0.7151	1.0301	0.9386
0.0313	0.4778	0.9046	0.6280	0.4787	0.9082	0.6305	0.6288	0.9057	0.8269
0.0294	0.4233	0.8016	0.5566	0.4244	0.8046	0.5590	0.5572	0.8025	0.7351
0.0278	0.3777	0.7153	0.4966	0.3789	0.7181	0.4989	0.4971	0.7160	0.6542
0.0263	0.3391	0.6422	0.4459	0.3397	0.6441	0.4472	0.4462	0.6428	0.5892
0.0250	0.3061	0.5797	0.4025	0.3065	0.5820	0.4037	0.4028	0.5802	0.5275
0.0238	0.2777	0.5259	0.3652	0.2782	0.5270	0.3660	0.3654	0.5263	0.4826
0.0227	0.2530	0.4793	0.3328	0.2535	0.4809	0.3334	0.3330	0.4796	0.4388
$R=\frac{h}{L}$		$V_0^{cr}(mv)$			$V_0^{cr}(mv)$			$V_0^{cr}(mv)$	
0.0385	88.13	166.77	115.78	88.60	167.96	116.93	115.99	167.09	152.92
0.0357	76.04	143.91	99.92	76.32	144.56	100.53	100.07	144.15	131.56
0.0333	66.27	125.44	87.09	66.50	126.31	87.47	87.21	125.63	114.46
0.0313	58.26	110.31	76.59	58.38	110.76	76.89	76.68	110.45	100.84
0.0294	51.63	97.76	67.87	51.75	98.13	68.17	67.95	97.87	89.65
0.0278	46.06	87.23	60.56	46.20	87.58	60.84	60.62	87.32	79.78
0.0263	41.35	78.31	54.37	41.43	78.54	54.54	54.42	78.39	71.86
0.0250	37.32	70.70	49.09	37.38	70.98	49.23	49.12	70.76	64.33
0.0238	33.86	64.14	44.53	33.93	64.27	44.64	44.56	64.19	58.85
0.0227	30.86	58.45	40.58	30.92	58.64	40.66	40.61	58.49	53.52
$R=\frac{h}{L}$		$\Delta T^{cr}(\dot{C})$			$\Delta T^{cr}(\dot{C})$			$\Delta T^{cr}(\dot{C})$	
0.0385	602	1140	791	605	1148	799	793	1142	1045
0.0357	520	983	683	521	988	687	684	985	899
0.0333	453	857	595	454	863	598	596	858	782
0.0313	398	754	523	399	757	525	524	755	689
0.0294	353	668	464	354	671	466	464	669	613
0.0278	315	596	414	316	598	416	414	597	545
0.0263	283	535	372	283	537	373	372	536	491
0.0250	255	483	335	255	485	336	336	484	440
0.0238	231	438	304	232	439	305	305	439	402
0.0227	211	399	277	211	401	278	277	400	366

Analysis of the buckling behavior of the sandwich nano-beams with FG-CNTRC face-sheets was implemented in this investigation. The nonlocal strain gradient elasticity theory and different higher order shear deformation beam theories were simultaneously considered for calculation of critical buckling load. In order to include coupling of strain and electrical field, the nonlocal non-classical nano-beam model involved piezoelectric effect. After solving the governing equations by DQM, the critical mechanical load, critical voltage and critical temperature rising were calculated. Then, the influences of some main parameters such as the effects of important parameters such as various HSDBTs, small scales parameter, volume fraction of the CNTs, foundation parameters, various boundary conditions, the CNTs efficiency parameter, and geometric dimensions on the buckling behaviors of FG sandwich nano-beam were studied in detail. The most important results of this study are presented as:

1. According to results, the mechanical critical load, critical voltage and critical temperature rising of the sandwich nano-beam were significantly decreased by increasing/decreasing the nonlocal parameter/the small scale parameter (strain gradient parameter). It means that considering the nonlocal and strain gradient parameters led

Table 9 the Mechanical Critical load for different CNTs efficiency parameter and volume fraction in face-sheets with varying critical buckling electrical load

	TSDBT, UU Pattern & $V_{cn} = 0.17,\ \eta = 0.142$			TSDBT, UU Pattern & $V_{cn} = 0.12,\ \eta = 0.137$			TSDBT, UU Pattern & $V_{cn} = 0.28,\ \eta = 0.141$		
	S_S	S_C	C_C	S_S	S_C	C_C	S_S	S_C	C_C
N_e		N_m^{cr}			N_m^{cr}			N_m^{cr}	
4.133	5.2253	6.3372	8.3590	4.9838	5.8520	7.4336	5.7018	7.2932	10.1785
4.216	5.3076	6.4192	8.4404	5.0661	5.9340	7.5150	5.7841	7.3752	10.2599
4.298	5.3899	6.5012	8.5218	5.1484	6.0160	7.5964	5.8664	7.4572	10.3413
4.381	5.4722	6.5832	8.6031	5.2308	6.0980	7.6777	5.9487	7.5392	10.4226
4.463	5.5546	6.6652	8.6845	5.3131	6.1800	7.7591	6.0311	7.6212	10.5040
4.546	5.6369	6.7472	8.7659	5.3954	6.2620	7.8405	6.1134	7.7031	10.5854
4.629	5.7192	6.8292	8.8473	5.4778	6.3440	7.9219	6.1957	7.7851	10.6668
4.711	5.8016	6.9112	8.9286	5.5601	6.4260	8.0033	6.2781	7.8671	10.7482
4.794	5.8839	6.9932	9.0100	5.6424	6.5080	8.0846	6.3604	7.9491	10.8295
4.877	5.9662	7.0752	9.0914	5.7248	6.5900	8.1660	6.4427	8.0311	10.9109

Table 10 the Mechanical Critical load for different CNTs efficiency parameter and volume fraction in face-sheets with varying Winkler parameter of elastic foundation

	ASDBT, VA Pattern, $V_{cn} = 0.17,\ \eta = 0.142$ & S_S boundary condition			ASDBT, UU Pattern, $V_{cn} = 0.17,\ \eta = 0.142$ & S_S boundary condition			ASDBT, AV Pattern, $V_{cn} = 0.17,\ \eta = 0.142$ & S_S boundary condition		
	$N_T = 0$	$N_T = 0.0654$	$N_T = 0.1307$	$N_T = 0$	$N_T = 0.0654$	$N_T = 0.1307$	$N_T = 0$	$N_T = 0.0654$	$N_T = 0.1307$
K_w		N_m^{cr}			N_m^{cr}			N_m^{cr}	
0.0183	2.0469	1.9818	1.9167	2.5370	2.4149	2.2928	1.7813	1.7162	1.6511
0.022	2.2336	2.1686	2.1034	2.7238	2.6017	2.4795	1.9681	1.9030	1.8379
0.0256	2.4204	2.3553	2.2902	2.9105	2.7884	2.6663	2.1548	2.0897	2.0246
0.0293	2.6072	2.5421	2.4769	3.0973	2.9752	2.8530	2.3416	2.2765	2.2114
0.033	2.7939	2.7288	2.6637	3.2841	3.1619	3.0398	2.5284	2.4633	2.3981
0.0366	2.9807	2.9156	2.8504	3.4708	3.3487	3.2265	2.7151	2.6500	2.5849
0.0403	3.1674	3.1023	3.0372	3.6576	3.5354	3.4133	2.9019	2.8368	2.7717
0.0439	3.3542	3.2891	3.2240	3.8443	3.7222	3.6001	3.0886	3.0235	2.9584
0.0476	3.5410	3.4758	3.4107	4.0311	3.9089	3.7868	3.2754	3.2103	3.1452
0.0513	3.7277	3.6626	3.5975	4.2178	4.0957	3.9736	3.4621	3.3970	3.3319

Table 11 the Mechanical Critical load for different $\frac{h_f}{h_H}$ ratio and CNTs volume fraction in face-sheets with varying Pasternak parameter of elastic foundation

	ASDBT, UU Pattern, $V_{cn} = 0.17,\ \eta = 0.142$ & C_C boundary condition			ASDBT, UU Pattern, $V_{cn} = 0.12,\ \eta = 0.137$ & C_C boundary condition			ASDBT, UU Pattern, $V_{cn} = 0.28,\ \eta = 0.141$ & C_C boundary condition		
	$\frac{h_f}{h_H} = \frac{1}{2}$	$\frac{h_f}{h_H} = \frac{3}{4}$	$\frac{h_f}{h_H} = 1$	$\frac{h_f}{h_H} = \frac{1}{2}$	$\frac{h_f}{h_H} = \frac{3}{4}$	$\frac{h_f}{h_H} = 1$	$\frac{h_f}{h_H} = \frac{1}{2}$	$\frac{h_f}{h_H} = \frac{3}{4}$	$\frac{h_f}{h_H} = 1$
K_s		N_m^{cr}			N_m^{cr}			N_m^{cr}	
0.0007	6.7804	7.1478	7.3152	5.2216	5.4703	5.5835	9.8568	10.4609	10.7359
0.0008	6.8804	7.2478	7.4152	5.3216	5.5703	5.6835	9.9568	10.5608	10.8359
0.0009	6.9804	7.3478	7.5152	5.4216	5.6703	5.7835	10.0568	10.6608	10.9359
0.0011	7.0804	7.4478	7.6152	5.5216	5.7703	5.8835	10.1568	10.7609	11.0359
0.0012	7.1804	7.5478	7.7152	5.6216	5.8703	5.9835	10.2568	10.8609	11.1359
0.0013	7.2804	7.6478	7.8152	5.7216	5.9703	6.0835	10.3568	10.9608	11.2359
0.0015	7.3804	7.7478	7.9152	5.8216	6.0703	6.1835	10.4568	11.0608	11.3359
0.0016	7.4804	7.8478	8.0152	5.9216	6.1703	6.2835	10.5568	11.1608	11.4359
0.0017	7.5804	7.9478	8.1152	6.0216	6.2703	6.3835	10.6568	11.2608	11.5359
0.0019	7.6804	8.0478	8.2152	6.1216	6.3703	6.4835	10.7568	11.3608	11.6359

Table 12 the Mechanical Critical load for different small scale theories and HOSDBTs with varying Winkler parameter of elastic foundation

	FSDBT, UU & C_C			TSDBT, UU & C_C			TSDBT, UU & C_C		
	CET	NET	NSGET	CET	NET	NSGET	CET	NET	NSGET
K_w		N_m^{cr}			N_m^{cr}			N_m^{cr}	
0.012	2.295	2.263	2.269	2.292	2.259	2.265	2.292	2.259	2.265
0.015	2.482	2.449	2.456	2.479	2.446	2.452	2.479	2.446	2.452
0.017	2.669	2.636	2.642	2.665	2.633	2.639	2.666	2.633	2.639
0.020	2.856	2.823	2.829	2.852	2.819	2.826	2.852	2.820	2.826
0.022	3.043	3.010	3.016	3.039	3.006	3.012	3.039	3.006	3.013
0.024	3.229	3.196	3.203	3.226	3.193	3.199	3.226	3.193	3.199
0.027	3.416	3.383	3.389	3.412	3.380	3.386	3.413	3.380	3.386
0.029	3.603	3.570	3.576	3.599	3.566	3.573	3.599	3.567	3.573
0.032	3.790	3.757	3.763	3.786	3.753	3.759	3.786	3.753	3.760
0.034	3.976	3.943	3.950	3.973	3.940	3.946	3.973	3.940	3.946

to decrease/increase the bending stiffness of the sandwich nano-beams. Regarding to differences between buckling loads obtained with and without considering small scale effects indicate aforementioned parameters have significant influences on buckling behavior of the sandwich nano-beams with FG-CNTRC face-sheets.

2. One of the main results that can be deduced form the results is the amounts of the critical buckling mechanical load calculated by PSDBT and TSDBT approximately have same values as well as ESDBT and ASDBT. Also, it is worthy noted that buckling load calculated by aforementioned theories was nearly smaller than buckling load estimated by FSDBT.

3. Numerical results indicate that distribution patterns have main effects on buckling behavior of sandwich nano-beams. Regarding to obtained results UU CNTs distribution pattern has the largest critical buckling mechanical load, critical buckling applied voltage and critical buckling temperature increment.

4. In accordance to the results, it is worthy noted that with increasing the Winkler foundation, the buckling mechanical load increased. In addition, the mechanical buckling load decreased by enhancing simultaneously thermal load.

5. Regarding to results, it concluded that enhancing the volume fraction of CNTs in face-sheets and efficiency parameter led to increase of the buckling mechanical load. In addition, if buckling mechanical load and electrical load are simultaneously applied on sandwich nano-beam, the increase of electrical load led to decrease the buckling mechanical load.

6. Geometric dimensions of the sandwich nano-beam can strongly change the critical buckling load. The results indicate that Enhancing the $\frac{h_f}{h_H}$ ratio and Pasternak coefficient led to increase of the mechanical buckling load in whole of the volume fraction of CNTs in face-sheets and efficiency parameter.

References

Allahkarami, F., Nikkhah-Bahrami, M. and Ghassabzadeh Saryazdi, M. (2017), "Damping and vibration analysis of viscoelastic curved microbeam reinforced with FG-CNTs resting on viscoelastic medium using strain gradient theory and DQM", *Steel Compos. Struct.*, **25**(2), 141-155.

Ansari, R., Faghih Shojaei, M., Mohammadi, V., Gholami, R. and Sadeghi, S. (2014), "Nonlinear forced vibration analysis of functionally graded carbon nanotube-reinforced composite Timoshenko beams", *Compos. Struct.*, **113**, 316-327.

Ansari, R., Gholami, R., Faghih Shojaei, M., Mohammadi, V. and Darabi, M.A. (2016), "Coupled longitudinal-transverse-rotational free vibration of post-buckled functionally graded first-order shear deformable micro- and nano-beams based on the Mindlin's strain gradient theory", *Appl. Math. Modell.*, **40**(23-24), 9872-9891.

Ansari, R. and Sahmani, S. (2011), "Bending behavior and buckling of nanobeams including surface stress effects corresponding to different beam theories", *Int. J. Eng. Sci.*, **49**(11), 1244-1255.

Arefi, M. (2016), "Analysis of wave in a functionally graded magneto-electro-elastic nano-rod using nonlocal elasticity model subjected to electric and magnetic potentials", *Acta Mech.* **227**(9), 2529-2542.

Arefi, M., Zamani, M.H. and Kiani, M. (2017), "Size-dependent free vibration analysis of three-layered exponentially graded nanoplate with piezomagnetic face-sheets resting on Pasternak's foundation", *J. Intel. Mater. Syst. Struct.*, **29**(5), 774-786

Arefi, M. and Zenkour, A.M. (2017a), "Employing the coupled stress components and surface elasticity for nonlocal solution of wave propagation of a functionally graded piezoelectric Love nanorod model", *J. Intel. Mater. Syst. Struc.*, **28**(17), 2403-2413.

Arefi, M. and Zenkour, A.M. (2017b), "Transient sinusoidal shear deformation formulation of a size-dependent three-layer piezo-magnetic curved nanobeam", *Acta. Mech.*, **228**(10) 3657-3674.

Arefi, M. and Zenkour, A.M. (2017c) "Influence of magneto-electric environments on size-dependent bending results of three-layer piezomagnetic curved nanobeam based on sinusoidal shear deformation theory", *J. Sandw. Struct. Mater.*, In Press.

Arefi, M. and Zenkour, A.M. (2017d), "Electro-magneto-elastic analysis of a three-layer curved beam", *Smart Struct. Syst.*, **19**(6), 695-703.

Arefi, M. and Zenkour, A.M. (2017e), "Size-dependent free vibration and dynamic analyses of piezo-electro-magnetic sandwich nanoplates resting on viscoelastic foundation", *Phys. B.*, **521**, 188-197.

Arefi, M. and Zenkour, A.M. (2017f), "Effect of thermo-magneto-electro-mechanical fields on the bending behaviors of a three-layered nanoplate based on sinusoidal shear-deformation plate theory", *J. Sandw. Struct. Mater.*, In Press.

Arvin, H., Sadighi, M. and Ohadi, A.R. (2010), "A numerical study of free and forced vibration of composite sandwich beam with viscoelastic core", *Compos. Struct.*, **92**(4), 996-1008.

Asghari, M., Kahrobaiyan, M.H. and Ahmadian, M.T. (2010), "A nonlinear Timoshenko beam formulation based on the modified couple stress theory", *Int. J. Eng. Sci.*, **48**(12), 1749-1761.

Belabed, Z., Houari, M.S.A., Tounsi, A., Mahmoud, S.R. and Anwar Bég, O. (2014), "An efficient and simple higher order shear and normal deformation theory for functionally graded material (FGM) plates", *Compos.: Part B*, **60**, 274-283.

El-HakimKhalil, A., E., E., Atta, A. and Essam, M. (2016), "Nonlinear behavior of RC beams strengthened with strain hardening cementitious composites subjected to monotonic and cyclic loads", *Alexandr. Eng. J.*, **55**(2), 1483-1496.

Eltaher, M.A., Khater, M.E. and Emam, S.A. (2016), "A review on nonlocal elastic models for bending, buckling, vibrations, and wave propagation of nanoscale beams", *Appl. Math. Modell.*, **40**(5-6), 4109-4128.

Fantuzzi, N., Tornabene, F., Bacciocchi, M. and Dimitri, R. (2017), "Free vibration analysis of arbitrarily shaped functionally graded carbon nanotube-reinforced plates", *Compos. Part B: Eng.*, **115**, 384-408.

Ghasemi, H., Park, H.S. and Rabczuk, T. (2017), "A level-set based IGA formulation for topology optimization of flexoelectric materials", *Comput. Met. Appl. Mech. Eng.*, **313**, 239-258.

Ghasemi, H., Park, H.S. and Rabczuk, T. (2018), "A multi-material level set-based topology optimization of flexoelectric composites", *Comput. Meth. Appl. Mech. Eng.*, **332**, 47-62.

Ghorbanpour Arani, A., Kolahchi, R., Mosallaie Barzoki, A.A., Mozdianfard, M.R. and Noudeh Farahani, M. (2012), "Elastic foundation effect on nonlinear thermo-vibration of embedded double-layered orthotropic graphene sheets using differential quadrature method", *Proc. IMechE Part C: J. Mech. Eng. Sci.*, 1-18.

Ghorbanpour Arani, A., Kolahchi, R. and Vossough, H. (2012), "Buckling analysis and smart control of SLGS using elastically coupled PVDF nanoplate based on the nonlocal Mindlin plate theory", *Phys. B*, **407**(22), 4458-4465.

Ghorbanpour Arani, A., Vossough, H., Kolahchi, R. and Mosallaie Barzoki, A.A. (2012), "Electro-thermo nonlocal nonlinear vibration in an embedded polymeric piezoelectric micro plate reinforced by DWBNNTs using DQM", *J. Mech. Sci. Technol.*, **26**(10), 3047~3057.

Grygorowicz, M., Magnucki, K. and Malinowski, M. (2015), "Elastic buckling of a sandwich beam with variable mechanical properties of the core", *Thin-Wall. Struct.*, **87**, 127-132.

Gui-Lin, S., Fuh-Gwo, Y. and Yi-Ru, R. (2017), "Thermal buckling and post-buckling analysis of functionally graded beams based on a general higher-order shear deformation theory", *Appl. Math. Modell.*, **47**, 340-357.

Hamdi, K.M., Silani, M., Zhuang, X., He, P. and Rabczuk, T. (2017), "Stochastic analysis of the fracture toughness of polymeric nanoparticle composites using polynomial chaos expansions", *Int. J. Fract.*, **206**(2), 215-227.

Hamdia, K.M., Silani, M., Zhuang, X., He, P. and Rabczuk, T. (2017), "Stochastic analysis of the fracture toughness of polymeric nanoparticle composites using polynomial chaos expansions", *Int. J. Fract.*, **206**(2), 215–227.

Hebali, H., Tounsi, A., Houari, M.S.A., Bessaim, A. and Adda Bedia, E.A. (2014), "A new quasi-3D hyperbolic shear deformation theory for the static and free vibration analysis of functionally graded plates", *ASCE J Eng. Mech.*, **140**(2), 374-383.

Kameswara Raoa, C. and Bhaskara Rao, L. (2017), "Torsional post-buckling of thin-walled open section clamped beam supported on Winkler-Pasternak foundation", *Thin-Wall. Struct.*, **116**, 320-325.

Kanani, A.S., Niknam, H., Ohadi, A.R. and Aghdam, M.M. (2014), "Effect of nonlinear elastic foundation on large amplitude free and forced vibration of functionally graded beam", *Compos. Struct.*, **115**, 60-68.

Ke, L.L., Yang, J. and Kitipornchai, S. (2010), "Nonlinear free vibration of functionally graded carbon nanotube-reinforced composite beams", *Compos. Struct.*, **92**(3), 676-683.

Komijani, M., Esfahani, S.E., Reddy, J.N., Liu, Y.P. and Eslami, M.R. (2014), "Nonlinear thermal stability and vibration of pre/post-buckled temperature-and microstructure-dependent functionally graded beams resting on elastic foundation", *Compos. Struct.*, **112**, 292-307.

Li, J., Wu, Z., Kong, X., Li, X. and Wu, W. (2014), "Comparison of various shear deformation theories for free vibration of laminated composite beams with general lay-ups", *Compos. Struct.*, **108**, 767-778.

Li, L. and Hu, Y. (2016), "Wave propagation in fluid-conveying viscoelastic carbon nanotubes based on nonlocal strain gradient theory", *Comput. Mater. Sci.*, **112**, 282-288.

Li, L., Hu, Y. and Ling, L. (2015), "Wave propagation in viscoelastic single-walled carbon nanotubes with surface effect under magnetic field based on nonlocal strain gradient theory", *Phys. E*, **75**, 118-124.

Liew, K.M., Yang, J. and Kitipornchai, S. (2003), "Postbuckling of piezoelectric FGM plates subject to thermo-electro-mechanical loading", *Int. J. Sol. Struct.*, **40**(15), 3869-3892.

Madani, H., Hosseini, H. and Shokravi, M. (2016), "Differential cubature method for vibration analysis of embedded FG-CNT-reinforced piezoelectric cylindrical shells subjected to uniform and non-uniform temperature distributions", *Steel Compos. Struct.*, **22**(4), 889-913.

Mahi, A., Adda Bedia, E.A. and Tounsi, A. (2015), "A new hyperbolic shear deformation theory for bending and free vibration analysis of isotropic, functionally graded, sandwich and laminated composite plates", *Appl. Math. Modell.*, **39**(9), 2489-2508.

Marzbanrad, J., Boreiry, M. and Shaghaghi, G.R. (2017), "Surface effects on vibration analysis of elastically restrained piezoelectric nanobeams subjected to magneto-thermo-electrical field embedded in elastic medium", *Appl. Phys. A.*, **123**(4), 246.

Meiche, N.E., Tounsi, A., Ziane, N., Mechab, I. and Adda Bedia, E.A. (2011), "A new hyperbolic shear deformation theory for buckling and vibration of functionally graded sandwich plate", *Int. J. Mech. Sci.*, **53**(4), 237-247.

Mirzabeigy, A. and Madoliat, R. (2016), "Large amplitude free vibration of axially loaded beams resting on variable elastic foundation", *Alexandr. Eng. J.*, **55**(2), 1107-1114.

Mohammadi, M., Farajpour, A., Moradi, A. and Ghayour, M. (2014), "Shear buckling of orthotropic rectangular graphene sheet embedded in an elastic medium in thermal environment", *Compos.: Part B*, **56**, 629-637.

Mohammadimehr, M., Rousta Navi, B. and Ghorbanpour Arani, A. (2016), "Modified strain gradient Reddy rectangular plate model for biaxial buckling and bending analysis of double-coupled piezoelectric polymeric nanocomposite reinforced by FG-SWNT", *Compos. Part B: Eng.*, **87**(15), 132-148.

Msekh, M.A., Cuong, N.H., Zi, G., Areias, P., Zhuang, X. and Rabczuk, T. (2018), "Fracture properties prediction of clay/epoxy nanocomposites with interphase zones using a phase field model", *Eng. Fract. Mech.*, **188**, 287-299.

Murmu, T. and Pradhan, S.C. (2009), "Buckling analysis of a single-walled carbon nanotube embedded in an elastic medium based on nonlocal elasticity and Timoshenko beam theory and using DQM", *Phys. E*, **41**(7), 1232-1239.

Murmu, T., Sienz, J., Adhikari, S. and Arnold, C. (2013), "Nonlocal buckling of double-nanoplate-systems under biaxial compression", *Compos.: Part B*, **44**(1), 84-94.

Natarajan, S., Haboussi, M. and Manickam, G. (2014), "Application of higher-order structural theory to bending and free vibration analysis of sandwich plates with CNT reinforced composite", *Compos. Struct.*, **113**, 197-207.

Niknam, H. and Aghdam, M.M. (2015), "A semi analytical approach for large amplitude free vibration and buckling of nonlocal FG beams resting on elastic foundation", *Compos. Struct.*, **119**, 452-462.

Rabani Bidgoli, M., Karimi, M.S. and Ghorbanpour Arani, A. (2015), "Viscous fluid induced vibration and instability of FG-CNT-reinforced cylindrical shells integrated with piezoelectric layers", *Steel Compos. Struct.*, **19**(3), 713-733.

Rafiee, M., He, X.Q. and Liew, K.M. (2014), "Non-linear dynamic stability of piezoelectric functionally graded carbon nanotube-reinforced composite plates with initial geometric imperfection", *Int. J. Non-Lin. Mech.*, **59**, 37-51.

Rafiee, M., Yang, J. and Kitipornchai, S. (2013), "Large amplitude vibration of carbon nanotube reinforced functionally graded composite beams with piezoelectric layers", *Compos. Struct.*, **96**, 716-725.

Rahmani, O., Hosseini, S.A.H., Ghoytasi, I. and Golmohammadi, H. (2017), "Buckling and free vibration of shallow curved micro/nano-beam based on strain gradient theory under thermal loading with temperature-dependent properties", *Appl. Phys. A.*, **123**(1), 4.

Reddy, J.N. (2007), "Nonlocal theories for bending, buckling and vibration of beams", *Int. J. Eng. Sci.*, **45**(2-8), 288-307.

Reddy, J.N. (2011), "Microstructure-dependent couple stress theories of functionally graded beams", *J. Mech. Phys. Sol.*, **59**(11), 2382-2399.

Reddy, J.N. and El-Borgi, S. (2014), "Eringen's nonlocal theories of beams accounting for moderate rotations", *Int. J. Eng. Sci.*, **82**, 159-177.

Shafiei, N. and Kazemi, M. (2017), "Buckling analysis on the bi-dimensional functionally graded porous tapered nano-/micro-scale beams", *Aerosp. Sci. Technol.*, **66**, 1-11.

Shen, H.S. and Zhang, C.L. (2012), "Non-linear analysis of functionally graded fiber reinforced composite laminated plates, part I: Theory and solutions", *Int. J. Non-Lin. Mech.*, **47**(9), 1045-1054.

Simsek, M. and Reddy, J.N. (2013), "Bending and vibration of functionally graded microbeams using a new higher order beam theory and the modified couple stress theory", *Int. J. Eng. Sci.*, **64**, 37-53.

Simsek, M. and Reddy, J.N. (2013), "A unified higher order beam theory for buckling of a functionally graded microbeam embedded in elastic medium using modified couple stress theory", *Compos. Struct.*, **101**, 47-58.

Simsek, M. and Yurtcu, H.H. (2013), "Analytical solutions for bending and buckling of functionally graded nanobeams based on the nonlocal Timoshenko beam theory", *Compos. Struct.*, **97**, 378-386.

Talebi, H., Silani, M., Bordas, S.P.A., Kerfriden, P. and Rabczuk, T. (2014), "A computational library for multiscale modeling of material failure", *Comput. Mech.*, **53**(5), 1047-1071.

Tornabene, F., Bacciocchi, M., Fantuzzi, N. and Reddy, J.N. "Multiscale approach for three-phase CNT/polymer/fiber laminated nanocomposite structures", In Press.

Tornabene, F., Fantuzzi, N. and Bacciocchi, M. (2014), "The strong formulation finite element method: Stability and accuracy", *Frattura ed Integrità Strutturale*, **8**(29), 251-265.

Tornabene, F., Fantuzzi, N. and Bacciocchi, M. (2017), "Linear static response of nanocomposite plates and shells reinforced by agglomerated carbon nanotubes", *Compos. Part B: Eng.*, **115**, 449-476.

Tornabene, F., Fantuzzi, N., Bacciocchi, M. and Viola, E. (2016), "Effect of agglomeration on the natural frequencies of functionally graded carbon nanotube-reinforced laminated composite doubly-curved shells", *Compos. Part B: Eng.*, **89**, 187-218.

Tornabene, F., Fantuzzi, N., Ubertini, F. and Viola, E. (2014), "Strong formulation finite element method based on differential quadrature: A survey", *Appl. Mech. Rev.*, **67**(2), 020801-020801-020855.

Tounsi, A., Houari, M.S.A., Benyoucef, S. and Adda Bedia, E.A. (2013), "A refined trigonometric shear deformation theory for thermoelastic bending of functionally graded sandwich plates", *Aerosp. Sci. Technol.*, **24**(1), 209-220.

Vu-Bac, N., Duong, T.X., Lahmer, T., Zhuang, X., Sauer, R.A., Park, H.S. and Rabczuk, T. (2018), "A NURBS-based inverse analysis for reconstruction of nonlinear deformations of thin shell structures", *Comput. Meth. Appl. Mech. Eng.*, **332**, 47-62.

Wattanasakulpong, N. and Ungbhakorn, V. (2013), "Analytical solutions for bending, buckling and vibration responses of carbon nanotube-reinforced composite beams resting on elastic foundation", *Comput. Mater. Sci.*, **71**, 201-208.

Wu, H. and Kitipornchai, S. (2015), "Free vibration and buckling analysis of sandwich beams with functionally graded carbon nanotube-reinforced composite face sheets", *Int. J. Struct. Stab. Dyn.*, **15**(7), 1540011

Wu, H., Kitipornchai, S. and Yang, J. (2017), "Imperfection sensitivity of thermal post-buckling behaviour of functionally graded carbon nanotube-reinforced composite beams", *Appl. Math. Modell.*, **42**, 735-752.

Yas, M.H. and Samadi, N. (2012), "Free vibrations and buckling analysis of carbon nanotube-reinforced composite Timoshenko beams on elastic foundation", *Int. J. Press. Vess. Pip.*, **98**, 119-128.

Zhu, X., Wang, Y. and Dai, H.H. (2017), "Buckling analysis of Euler-Bernoulli beams using Eringen's two-phase nonlocal model", *Int. J. Eng. Sci.*, **116**, 130-140.

Ziaee, S. (2016), "Steady state response of functionally graded nano-beams resting on viscous foundation to super-harmonic excitation", *Alexandr. Eng. J.*, **55**(3), 2655-2664.

Abbreviation

FG	functionally graded
CNTs	carbon nanotubes
PDE	partial differential equation
ODE	ordinary differential equation
UD	uniform distribution
SWCNT	single-walled carbon nanotube
CFs	carbon fibers
CNTRCs	carbon nanotube-reinforced composites

MEMS	micro-electro-mechanical systems
NEMS	nano-electro-mechanical systems
MLPG	meshless local Petrov-Galerkin

Appendix A

A1:

$$A_{x1}=\int_h\left(C_{11}(z)+\frac{e_{31}(z)^2}{a_{33}(z)}\right)dzb,\quad A_{x2}=\frac{1}{2}\int_h\left(-f_{111}(z)\frac{e_{31}(z)}{a_{33}(z)}\right)dzb,$$
$$B_{x1}=-\int_h\left(C_{11}(z)+\frac{e_{31}(z)^2}{a_{33}(z)}\right)zdzb, A_{x3}=\frac{1}{2}\int_h\left(-f_{14}(z)\frac{e_{31}(z)}{a_{33}(z)}\right)dzb,$$
$$B_{x2}=\int_h\left(C_{11}(z)+\frac{e_{31}(z)^2}{a_{33}(z)}\right)zdzb, B_{x2}=\frac{1}{2}\int_h\left(-f_{111}(z)\frac{e_{31}(z)}{a_{33}(z)}\right)zdzb, \tag{1}$$
$$B_{x3}=\frac{1}{2}\int_h\left(-f_{14}(z)\frac{e_{31}(z)}{a_{33}(z)}\right)zdzb,\ D_{x1}=-\int_h\left(C_{11}(z)+\frac{e_{31}(z)^2}{a_{33}(z)}\right)z^2dzb,$$

$$A^1_{131}=\frac{1}{2}\int_h\left(\frac{f_{111}(z)e_{31}(z)}{a_{33}(z)}\right)dzb,\ A^2_{131}=\frac{1}{2}\int_h\left(\frac{f_{111}(z)f_{14}(z)}{a_{33}(z)}+\frac{f_{111}(z)^2}{a_{33}(z)}\right)dzb,$$
$$A^3_{131}=\frac{1}{2}\int_h\left(\frac{f_{111}(z)f_{14}(z)}{a_{33}(z)}\right)dzb,\ B_{131}=\frac{1}{2}\int_h\left(\frac{f_{111}(z)e_{31}(z)}{a_{33}(z)}\right)zdzb,$$
$$A^1_{113}=\frac{1}{2}\int_h\left(\frac{f_{14}(z)e_{31}(z)}{a_{33}(z)}\right)dzb,\ A^2_{113}=\frac{1}{2}\int_h\left(\frac{f_{111}(z)f_{14}(z)}{a_{33}(z)}-\frac{f_{14}(z)^2}{a_{33}(z)}\right)dzb, \tag{2}$$
$$A^3_{113}=\frac{1}{2}\int_h\left(\frac{f_{14}(z)^2}{a_{33}(z)}\right)dzb,\qquad B_{113}=\frac{1}{2}\int_h\left(\frac{f_{14}(z)e_{31}(z)}{a_{33}(z)}\right)zdzb,$$

$$A^s{}_{x1}=\int_h\left(C^s{}_{11}(z)+\frac{e^s{}_{31}(z)e_{31}(z)}{a_{33}(z)}\right)dz+$$
$$\left[\left(C^s{}_{11}(z)+\frac{e^s{}_{31}(z)e_{31}(z)}{a_{33}(z)}\right)\Bigg|_{z=\frac{h}{2}}-\left(C^s{}_{11}(z)+\frac{e^s{}_{31}(z)e_{31}(z)}{a_{33}(z)}\right)\Bigg|_{z=-\frac{h}{2}}\right]\frac{h}{2},$$
$$A^s{}_{x2}=\frac{1}{2}\int_h\left(\frac{f_{111}(z)}{a_{33}(z)}+\frac{f_{14}(z)}{a_{33}(z)}\right)e^s{}_{31}(z)dz$$
$$\left[\left(\frac{f_{111}(z)}{a_{33}(z)}+\frac{f_{14}(z)}{a_{33}(z)}\right)e^s{}_{31}(z)\Bigg|_{z=\frac{h}{2}}-\left(\frac{f_{111}(z)}{a_{33}(z)}+\frac{f_{14}(z)}{a_{33}(z)}\right)e^s{}_{31}(z)\Bigg|_{z=-\frac{h}{2}}\right]\frac{h}{2}, \tag{3}$$
$$A^s{}_{x3}=\frac{1}{2}\int_h\left(f_{14}(z)\frac{e^s{}_{31}(z)}{a_{33}(z)}\right)dz+$$
$$\left[\left(\frac{e^s{}_{31}(z)f_{14}(z)}{a_{33}(z)}\right)\Bigg|_{z=\frac{h}{2}}-\left(\frac{e^s{}_{31}(z)f_{14}(z)}{a_{33}(z)}\right)\Bigg|_{z=-\frac{h}{2}}\right]\frac{h}{2},$$

$$B^s{}_{x1}=\int_h\left(C^s{}_{11}(z)-\frac{e^s{}_{31}(z)e_{31}(z)}{a_{33}(z)}\right)zdz+$$
$$\left[\left(C^s{}_{11}(z)-\frac{e^s{}_{31}(z)e_{31}(z)}{a_{33}(z)}\right)\Bigg|_{z=\frac{h}{2}}-\left(C^s{}_{11}(z)-\frac{e^s{}_{31}(z)e_{31}(z)}{a_{33}(z)}\right)\Bigg|_{z=-\frac{h}{2}}\right]\frac{bh^2}{2},$$
$$B^s{}_{x2}=\int_h\left(C^s{}_{11}(z)+\frac{e^s{}_{31}(z)e_{31}(z)}{a_{33}(z)}\right)zdz+ \tag{4}$$
$$\left[\left(C^s{}_{11}(z)+\frac{e^s{}_{31}(z)e_{31}(z)}{a_{33}(z)}\right)\Bigg|_{z=\frac{h}{2}}-\left(C^s{}_{11}(z)+\frac{e^s{}_{31}(z)e_{31}(z)}{a_{33}(z)}\right)\Bigg|_{z=-\frac{h}{2}}\right]\frac{bh^2}{2},$$

$$D^s{}_{x1}=\int_h\left(C^s{}_{11}(z)-\frac{e^s{}_{31}(z)e_{31}(z)}{a_{33}(z)}\right)z^2dz+$$
$$\left[\left(C^s{}_{11}(z)-\frac{e^s{}_{31}(z)e_{31}(z)}{a_{33}(z)}\right)\Bigg|_{z=\frac{h}{2}}-\left(C^s{}_{11}(z)-\frac{e^s{}_{31}(z)e_{31}(z)}{a_{33}(z)}\right)\Bigg|_{z=-\frac{h}{2}}\right]\frac{bh^3}{8},$$
$$B^s{}_{x3}=\frac{1}{2}\int_h\left(\frac{f_{111}(z)}{a_{33}(z)}+\frac{f_{14}(z)}{a_{33}(z)}\right)ze^s{}_{31}(z)dz$$
$$\left[\left(\frac{f_{111}(z)}{a_{33}(z)}+\frac{f_{14}(z)}{a_{33}(z)}\right)e^s{}_{31}(z)\Bigg|_{z=\frac{h}{2}}-\left(\frac{f_{111}(z)}{a_{33}(z)}+\frac{f_{14}(z)}{a_{33}(z)}\right)e^s{}_{31}(z)\Bigg|_{z=-\frac{h}{2}}\right]\frac{bh^2}{2}, \tag{5}$$
$$B^s{}_{x4}=\frac{1}{2}\int_h\left(f_{14}(z)\frac{e^s{}_{31}(z)}{a_{33}(z)}\right)zdz+$$
$$\left[\left(\frac{e^s{}_{31}(z)f_{14}(z)}{a_{33}(z)}\right)\Bigg|_{z=\frac{h}{2}}-\left(\frac{e^s{}_{31}(z)f_{14}(z)}{a_{33}(z)}\right)\Bigg|_{z=-\frac{h}{2}}\right]\frac{bh^2}{2},$$